

# Rational catalyst and electrolyte design for CO<sub>2</sub> electroreduction towards multicarbon products

Dunfeng Gao,<sup>1</sup> Rosa M. Arán-Ais,<sup>1</sup> Hyo Sang Jeon,<sup>1,2</sup> Beatriz Roldan Cuenya\*<sup>1</sup>

<sup>1</sup>Department of Interface Science, Fritz Haber Institute of the Max Planck Society, 14195 Berlin, Germany

<sup>2</sup>Department of Physics, Ruhr-University Bochum, 44780 Bochum, Germany

\*E-mail: roldan@fhi-berlin.mpg.de

This document is the unedited Author's version of a Submitted Work that was subsequently accepted for publication in Nature Catalysis, copyright © Springer Nature Limited after peer review. To access the final edited and published work see <https://www.nature.com/articles/s41929-019-0235-5>.

## Abstract

CO<sub>2</sub> electroreduction reaction (CO<sub>2</sub>RR) to fuels and feedstocks is an attractive route to close the anthropogenic carbon cycle and store renewable energy. The generation of more reduced chemicals, especially multicarbon oxygenate and hydrocarbon products (C<sub>2+</sub>) with higher energy density is highly desirable for industrial applications. However, selective conversion of CO<sub>2</sub> to C<sub>2+</sub> suffers from high overpotential, low reaction rate and low selectivity, and the process is extremely sensitive to the catalyst structure and electrolyte. Here we discuss strategies to achieve high C<sub>2+</sub> selectivity through rational design of the catalyst and electrolyte. Current state-of-the-art catalysts, including Cu and Cu-bimetallic catalysts as well as alternative materials are considered. The importance of taking into consideration the dynamic evolution of the catalyst structure and composition are highlighted, focusing on findings extracted from *in situ* and *operando* characterizations. Additional theoretical insight into the reaction mechanisms underlying the improved C<sub>2+</sub> selectivity of specific catalyst geometries/compositions in synergy with a well-chosen electrolyte are also provided.

Excessive CO<sub>2</sub> emissions from the utilization of traditional fossil energy sources cause severe environmental issues, hindering a sustainable development of our industrial society. The CO<sub>2</sub> electroreduction reaction (CO<sub>2</sub>RR) represents a viable alternative to help close the anthropogenic carbon cycle and convert intermittent electricity from renewable energy sources (i.e., solar, wind) to chemical energy in the form of fuels and feedstocks<sup>1-3</sup>. The most common products derived from CO<sub>2</sub>RR are CO and formic acid. However, the production of more reduced products such as multicarbon oxygenates and hydrocarbons (C<sub>2+</sub>) is highly desirable because of their higher energy density and wider applicability<sup>4,5</sup>. Such products are also of great significance from a point of view of fundamental research, since they involve the formation of the C-C bond, a key challenge in heterogeneous catalysis.

Extensive experimental and theoretical studies have focused on understanding the C-C coupling mechanism during the CO<sub>2</sub>RR. Although the initial activation of the stable CO<sub>2</sub> molecule is difficult, the binding strength of an intermediate \*CO (\* being an adsorption site) and its subsequent conversion via proton-electron transfer into the next hydrogenated species (e.g., \*CHO, \*COH, \*OCCO, \*OCCOH) on the catalyst surface determines whether H<sub>2</sub>, CO or more reduced oxygenates and hydrocarbons are formed as final products<sup>6,7</sup>. For the formation of C<sub>2+</sub> products, two pathways have been identified with regard to the C-C coupling step: (1) \*CO dimerizes to form \*OCCO species at low overpotentials<sup>8</sup>. (2) \*CO is hydrogenated to form \*CHO species,<sup>9</sup> a common intermediate for the formation of methane, which takes place at high overpotentials. The first pathway was recently confirmed by an *in situ* spectroscopic observation of the hydrogenated CO dimer intermediate (\*OCCOH) on the Cu(100) surface<sup>10</sup>. Differential electrochemical mass spectrometry (DEMS) measurements further revealed that acetaldehyde is an important intermediate for the formation of ethanol and propanol<sup>11,12</sup>. It should be noted that the C-C coupling step is highly sensitive to the structure of the catalyst and the electrolyte<sup>13</sup>. Cu is generally considered to be the only metal capable of producing hydrocarbons and oxygenates in significant amounts, but it still suffers from high overpotential, low C<sub>2+</sub> selectivity and concurrent hydrogen evolution reaction (HER). To access C<sub>2+</sub> products more efficiently, various nanostructured Cu catalysts have been developed by engineering low-coordinated sites and defects, by tuning the oxidation state, adding a secondary metal, or by modifying the size and shape of nanostructures<sup>14,15</sup>.

In this Review, we will discuss the current state-of-the-art Cu, Cu-bimetallic and some Cu-free catalysts towards the formation of C<sub>2+</sub> products from the CO<sub>2</sub>RR. The electrolyte effect on the catalyst structure before and during the reaction as well as on the CO<sub>2</sub>RR activity and selectivity will also be discussed. Information extracted from *in situ* and *operando* characterization methods<sup>16,17</sup> will be used to shed light into the reaction mechanism and the dynamic evolution of the catalysts under CO<sub>2</sub>RR conditions. Furthermore, the need of such studies in order to gain fundamental understanding of electrocatalytic processes will be prominently featured.

## Catalyst design: state-of-the-art catalysts for C<sub>2+</sub> products

Whether a catalyst can produce hydrocarbons and oxygenates, especially C<sub>2+</sub> products *via* C-C coupling, essentially depends on its structure and composition. Nanostructured Cu-based materials are the most popular catalysts for C<sub>2+</sub> products, while alternative non-Cu-based materials have also been explored. In this section we review the recent advances made in the development of these state-of-the-art catalysts and their mechanistic understanding with a special emphasis on the insights extracted from *in situ* and *operando* characterization methods.

**Cu nanoparticles (NPs).** Although Cu is an abundant and relatively cheap metal, maximizing the surface to volume ratio by using nanoparticulated catalysts is desirable for future implementation at the cathode of a CO<sub>2</sub> electrolyzer<sup>18,19</sup>. The special morphology of the NPs, together with their distinct electronic and chemical surface properties, usually confers improved catalytic activity compared to bulk materials. In this sense, the reactivity of NPs can be rationally tuned by modifying four fundamental parameters: size, shape, composition, and interparticle distance (or loading on the support). The NP size determines the density of low-coordinated atoms present at its surface, which can influence the binding strength of the different reaction intermediates, and thus affect the final product selectivity. In this sense, a size-dependent study on Cu NPs showed an increased activity but also enhanced selectivity towards H<sub>2</sub> and CO formation as the NP size decreased from 15 nm to 2 nm (Figure 1a). The latter results were linked to a greater population of low coordinated sites in smaller NPs (Figure 1b)<sup>20</sup> that favor HER versus CO<sub>2</sub>RR. An analogous trend was also seen for Au<sup>21,22</sup> and Zn<sup>23</sup> NPs and theoretically explained due to the weaker binding of reaction intermediates such as COOH\* to a NP surface covered by hydrogen<sup>16</sup>.

Higher activity and hydrocarbon/alcohol selectivity have been described for gas diffusion electrodes (GDE) and membrane electrode assemblies (MEA), for example, those in which large NPs (25 nm) were deposited, resulting in a higher ethylene production (1148 μmol m<sup>-2</sup> s<sup>-1</sup>) with an exceptionally high Faradaic efficiency (FE, 92.8 %) and suppression of the HER under galvanostatic conditions (j = 7.5 mA cm<sup>-2</sup>)<sup>24</sup>. These results bring into attention the importance of not only being able to fine-tune the catalytic material, but also the proper engineering of the different interfaces involved (gas/liquid/solid) for a better product selectivity at high current densities under practical reaction conditions. While catalyst integration into GDEs and MEAs is an emerging sub-field in CO<sub>2</sub>RR<sup>24,25</sup> the integration of *in situ* and *operando* characterization methods coupled with the GDE and MEA configurations is difficult and rarely reported. To deal with this issue, one could learn from the *in situ* techniques and cells developed for applications in water electrolysis systems and fuel cells. An example are X-ray absorption data acquired during real fuel cell and electrolyzer operation<sup>26-29</sup>. Nevertheless,

the implementation of surface-sensitive techniques is still a challenge due to the relatively thick gas diffusion layer present in front of the active catalyst in the GDE configuration.

Adjusting the distribution of a catalyst on a support is another strategy that has been followed to further modify the CO<sub>2</sub> product selectivity. In this sense, Cu NPs with narrow NP size distributions and uniform arrangement demonstrated an increasing selectivity towards methane and ethylene as the interparticle distance decreased, which was assigned to an enhanced reactant diffusion on the NP neighborhood and the re-adsorption of intermediate species<sup>30</sup>. Nevertheless, local changes in the pH for different NP arrangements may also be partially responsible for the experimental results observed. The NP areal density was also found crucial for the observation of an enhanced hydrocarbon selectivity<sup>31,32</sup> (Figure 1c). In the former systems, the larger electroactive surface area available appears to facilitate the stabilization and reaction between different adsorbed reaction intermediates. It was postulated that this fact, accompanied by the limited mass transport at the catalytic surface, as well as the proton depletion and higher local interfacial pH, enables the selective conversion of CO<sub>2</sub> to C<sub>2</sub>-C<sub>3</sub> hydrocarbons and oxygenates on highly packed Cu NP ensembles<sup>31,32</sup>. Interestingly, densely packed Cu NPs can undergo structural transformations during CO<sub>2</sub>RR into electrocatalytically more active cube-like particles capable of forming ethylene, ethanol, and n-propanol (Figure 1d)<sup>31</sup>. These results highlight the consequence of the dynamic structural and compositional changes experienced by Cu-based catalysts during CO<sub>2</sub>RR for the production of multicarbon products, and the need of cutting-edge characterization techniques based on *in situ* and *operando* microscopy and spectroscopy to further disentangle the parameters ruling electrocatalysts' activity and selectivity.

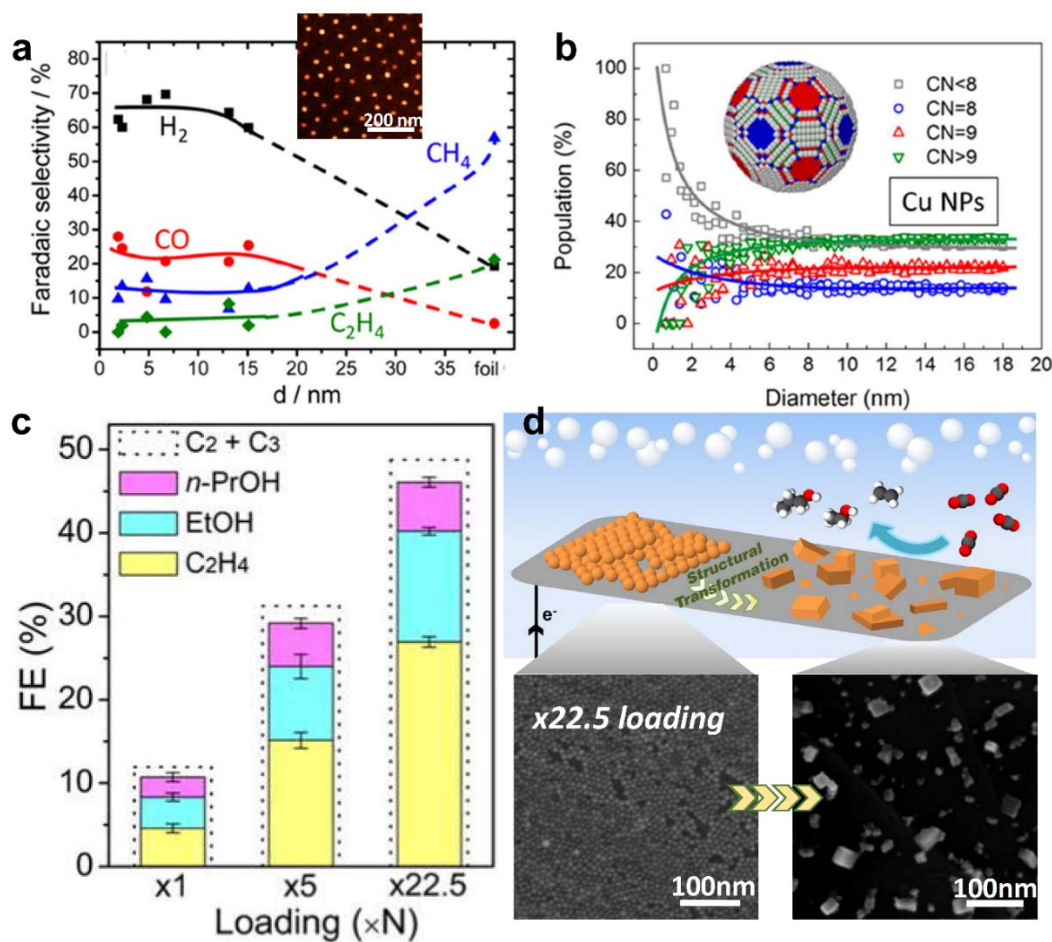


**Figure 1. NP size and loading effects.** **a.** Faradic selectivity as a function of Cu NP size in 0.1 M KHCO<sub>3</sub> electrolyte. The inset displays an AFM image of Cu NPs. **b.** Population of surface atoms with a specific coordination number as a function of the NP diameter with a schematic of a NP and its specifically coordinated surface atoms. **c.** Ethylene, ethanol, and n-propanol FE selectivity as a function of the Cu NP loading, with the dotted lines showing the overall C<sub>2</sub>-C<sub>3</sub> FE measured at -0.81 V vs RHE in a CO<sub>2</sub>-saturated 0.1 M KHCO<sub>3</sub> electrolyte. **d.** Schematic illustrating and SEM images of the *in situ* transformation process of the Cu NP ensembles to cubic-like structures. Figures adapted with permission from: **a-b** ref. <sup>20</sup>, American Chemical Society and **c-d** ref. <sup>31</sup>, American National Academy of Sciences.

**Cu model surfaces.** However, the wide surface heterogeneity of poly-oriented NPs makes difficult to extract clear correlations between the structural properties of the NPs and their reactivity. The use of model surfaces can serve to overcome this problem by being able to more directly extract information on the effect of surface structure on a given electrocatalytic reaction pathway. Accordingly, control over selectivity can be achieved by maximizing the exposure of the facets that have been previously proven more reactive for a certain process. Regarding CO<sub>2</sub>RR, preceding studies using Cu single crystal have shown that ethylene is selectively formed on Cu(100), while Cu(111) favors the formation of methane<sup>33,34</sup>. The presence of surface defects such as steps and/or kinks (i.e., undercoordinated sites) on

a well-ordered surface may also enhance the activity by modifying the surface binding energy of the adsorbates, thus changing the reaction pathway towards different products<sup>35,36</sup>. Theoretical studies, although still in an incipient stage due to the challenge associated with properly treating a complex electrode-electrolyte interface, have also devoted significant effort to unraveling the mechanism behind the different product selectivity on each surface orientation<sup>8,35,37,38</sup>. The most accepted theory so far proposed that the reaction pathway that yields to ethylene formation takes place via CO dimerization in a proton-decoupled one-electron reaction step, generating a  $C_2O_2^-$  intermediate that gets subsequently protonated<sup>8,38</sup>. In addition, the atomic square configuration of the Cu atoms on a (100) surface presents an optimal adsorption geometry for this dimer, and a better stabilization of the charged intermediate<sup>38</sup>. Later *in situ* experimental spectroscopic studies have revealed the hydrogenated CO dimer intermediate during CO electroreduction on Cu(100) (Figure 2a)<sup>10</sup> and also found that high surface coverage of adsorbed \*CO is essential for the selective formation of ethylene<sup>34</sup>. Furthermore, the dynamic changes of the surfaces, even in the case of single crystals under reaction conditions must be considered. Recent *quasi-operando* electrochemical scanning tunneling microscopy (EC-STM) and DEMS measurements demonstrated the transformation underwent by a Cu(polycrystalline)-to-Cu(100) reconstructed surface when subjected to oxidation-reduction cycles in a 0.1 M KOH solution<sup>39</sup>. The resulting ordered stepped surface, Cu(S) – [3(100) × (111)] or Cu(511) was found to reduce CO to ethanol at a lower overpotential and higher rate than the pristine Cu(100) surface. These results are in agreement with previous studies that reported the beneficial effect of (111) and (110) steps in (100) facets for the C–C bond formation<sup>33,40</sup>.

**Shape-controlled Cu nanocatalysts.** The surface structure sensitiveness of the CO<sub>2</sub>RR together with the aforementioned theoretical considerations hint towards the advantage of using NPs with controlled morphology to explore the so-called *facet effect* and prepare tailored materials with superior activity and selectivity. For example, by synthesizing cubic-shaped Cu nanostructures it is possible to guarantee the presence of well-ordered (100) domains while preserving the characteristic low-coordinated sites from NPs, morphology that has been demonstrated to lead to an increased ethylene selectivity and suppressed methane production<sup>41–43</sup>, especially when combined with Cu<sup>+</sup> and subsurface oxygen species<sup>44</sup>. The main drawback of these shape-selected nanocatalysts is their deactivation due to the loss of the well-defined facets and decrease in size under reaction conditions<sup>35</sup>. For instance, lower selectivity towards ethylene and ethanol in favor of methane production was found after the disappearance of the (100) facets on Cu nanocubes deposited on carbon (Figure 2b)<sup>45</sup>. In this study, *in situ* and *operando* techniques such as electrochemical atomic force microscopy (EC-AFM), X-ray absorption fine-structure spectroscopy (XAFS) and *quasi in situ* X-ray photoelectron spectroscopy (XPS) were crucial to correlate the changes in activity with the dynamic surface roughening, defect and pore formation, and CuO<sub>x</sub> reduction of the Cu nanocubes. Moreover, the lack of stability of Cu<sup>+</sup> species on the Cu cubes supported on C as compared to those grown on a Cu foil was also held responsible for the switch in the reaction selectivity from C<sub>2</sub>H<sub>4</sub> for Cu cubes/Cu to CH<sub>4</sub> for those deposited on carbon.

Other singular morphologies like highly porous 3D Cu dendrites and foams<sup>46-49</sup> have also shown high CO<sub>2</sub>RR activity and enhanced ethylene selectivity. However, since no preferential facet orientation prevails on these nanostructured materials, the high density of defects (steps, kinks and edges)<sup>50</sup>, grain boundaries<sup>51</sup> and surface roughness<sup>46,52</sup>, together with the concomitant changes in the interfacial pH<sup>53</sup>, are considered to be the parameters determining the resulting catalytic behavior. The residence time of the intermediates inside these 3D catalyst appears to be crucial for the C<sub>2</sub> products selectivity, as it was previously pointed out for ensembles of densely packed Cu NPs.

**Oxide-derived (OD) Cu catalysts.** Cu metal nanostructured surfaces derived from the *in situ* reduction of highly oxidized materials under CO<sub>2</sub>RR conditions also present unprecedented catalytic activity<sup>54</sup>, namely, lower onset potentials and enhanced selectivity toward C<sub>2+</sub> products over methane. Such trends have been assigned to their rough morphology and large defect density, also leading to changes in the local pH, as well as to possible changes of the chemical state of the active Cu species. In this sense, CO<sub>2</sub>RR has been lately studied on OD-Cu surfaces with different morphologies (nanoneedles, nanocrystals and NPs) using *operando* selected-ion flow tube mass spectrometry (SIFT-MS) and *in situ* Raman spectroscopy<sup>55</sup>. The results indicate that the reduction of Cu<sub>2</sub>O is energetically and kinetically favored compared to CO<sub>2</sub>RR, thus taking place before the selective generation of C<sub>2</sub> products<sup>45</sup>. Similar conclusions were extracted from the *ex situ* study of <sup>18</sup>O isotopically enriched OD-Cu catalysts, where the residual <sup>18</sup>O content found after CO<sub>2</sub>RR was neglectable<sup>56</sup>. However, recent reports have suggested that Cu<sup>+</sup> and residual subsurface oxygen might be at least partially responsible for the outstanding activity of Cu-OD catalysts<sup>27,57-60</sup>. According to theoretical simulations, the kinetics and thermodynamics of both, CO<sub>2</sub> activation and CO dimerization significantly improve due to the presence of subsurface oxygen<sup>58</sup> and Cu<sup>+</sup> and Cu<sup>0</sup> species at neighboring surface sites<sup>59</sup>, thereby increasing the efficiency and selectivity of CO<sub>2</sub>RR. Due to the rapid reoxidation of OD materials, the accuracy of *ex situ* measurements to determine the oxygen content is jeopardized, and *in situ* and *operando* methods are required. Experimental evidence of the survival of Cu<sup>+</sup> species during CO<sub>2</sub>RR was provided on plasma-oxidized Cu catalysts based on *operando* XAFS measurements. Interestingly, these catalysts displayed a high ethylene selectivity of 60 % at -0.9 V vs RHE<sup>57</sup>. The stabilization of Cu<sup>+</sup> has been recently achieved at Cu cube/Cu foil interfaces<sup>44,45</sup>, on CuO<sub>x</sub> foils by adding I<sup>-</sup> to the electrolyte<sup>61,62</sup>, or on porous dendritic nanostructures by using boron as a dopant (Cu(B)) to modify the electronic structure of Cu. In the later example, a conversion to C<sub>2</sub> products of up to 80 % FE at -1.1 V vs RHE and 40 h of initial sustained efficient operation (Figure 2C)<sup>60</sup> was reported. While one cannot neglect the role of the increased electrochemically active surface area (ECSA) of the highly roughened Cu catalysts in the reactivity trends obtained, the intrinsic activity cannot be simply determined by normalizing the current density by the ECSA<sup>63,64</sup>. In fact, such approach fails at considering the complexity of the catalytically active surface sites, which are not homogenous in nature. Therefore, it cannot be expected that every surface site would display an identical catalytic performance. It is well known in heterogeneous catalysis<sup>65</sup> that this is in fact not the case, and that at times, only a few surface sites dominate the catalytic

activity and selectivity trends. Nevertheless, in order to rule out the effect of the ECSA in CO<sub>2</sub>RR, control experiments should be conducted on samples with similar ECSA but where distinct active surface features (e.g. specific defects) are available<sup>44,57</sup>. Although the catalytic effect of Cu<sup>+</sup> and subsurface oxygen in Cu-based materials is a current topic of debate in electrocatalysis<sup>66</sup>, these results are promising and pave a way to finely tune Cu's properties towards higher activity and narrower product distribution.

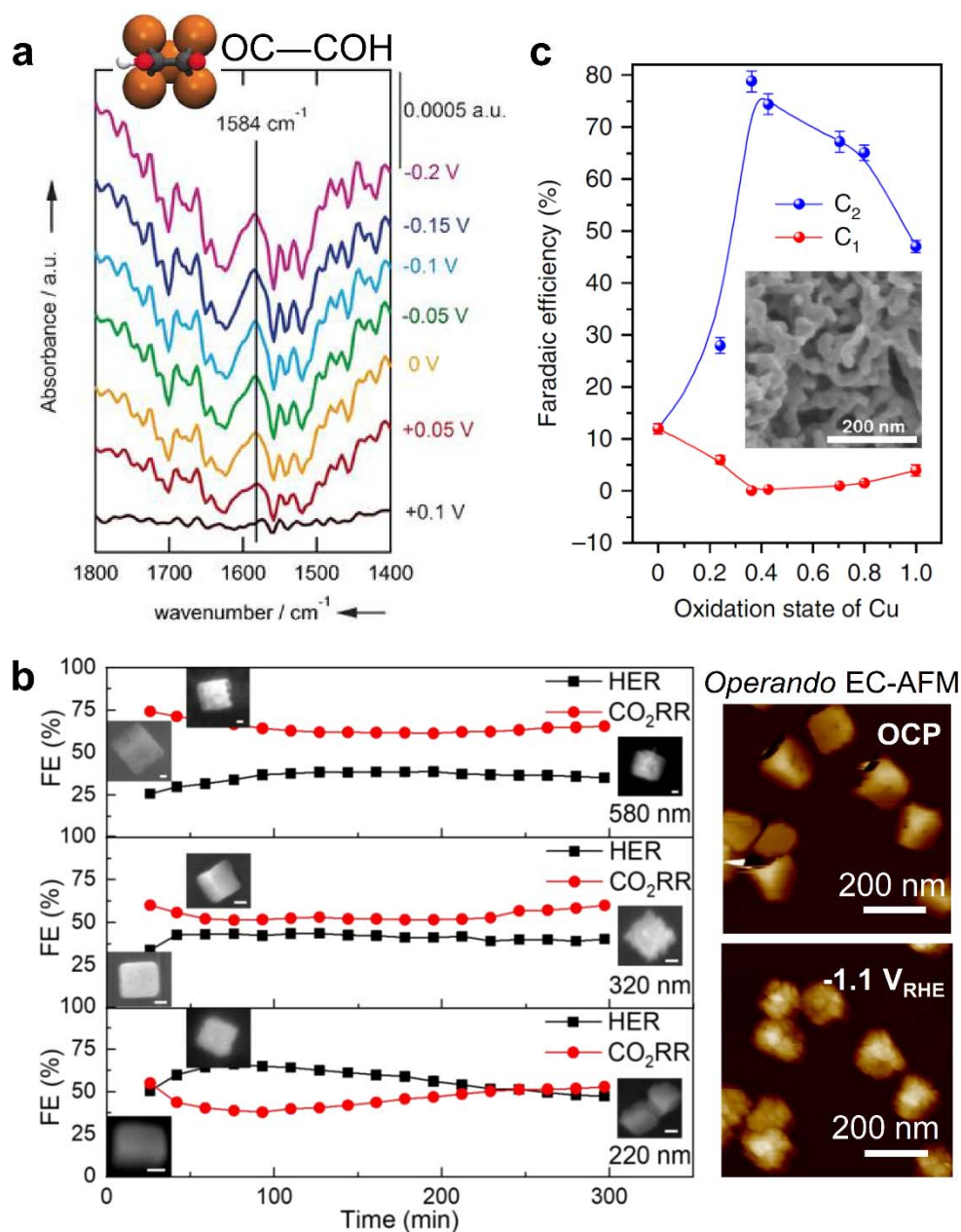


**Figure 2. Real time characterization of Cu-based catalysts. a.** Potential dependent absorbance spectra for Cu(100) in a 0.1 M LiOH solution using D<sub>2</sub>O as electrolyte. The highlighted band at 1584 cm<sup>-1</sup> corresponds to <sup>12</sup>C=O stretching from the adsorbed hydrogenated CO dimer (OCCOH) intermediate, as

depicted in the schematic structure. **b.** Faradic Efficiency for CO<sub>2</sub>RR and HER of samples with different Cu cube sizes (580 nm, 320 nm and 220 nm) recorded at  $-1.05$  V vs RHE during 5 h. The insets display SEM images of typical Cu cubes measured after different reaction times. The size of the scale bars is 100 nm. *Operando* EC-AFM images of  $\sim 100$  nm large Cu cubes acquired in 0.1 M KHCO<sub>3</sub> at open circuit potential (OCP) and at  $-1.1$  V vs RHE for 1 min. **c.** Faradaic Efficiency of C<sub>2</sub> and C<sub>1</sub> products obtained from Cu(B) samples with different Cu oxidation states tested at  $-1.1$  V vs RHE. The inset displays an SEM image of this material. Figures adapted with permission from: **a** ref. <sup>10</sup>, Wiley; **b** ref. <sup>45</sup>, Wiley and **c** ref. <sup>60</sup>, Nature Publishing Group.

**Cu-based bimetallic catalysts.** The formation of bimetallic alloys of Cu with various secondary metals is commonly used to alter the activity and selectivity of CO<sub>2</sub>RR. The catalytic performance of bimetallic catalysts for CO<sub>2</sub>RR varies as a function of their surface composition and structure, both of which might be modified during CO<sub>2</sub>RR. For instance, even when the same initial bimetallic composition is chosen (*e.g.*, CuPd bimetallic catalysts)<sup>67–70</sup>, different products may be produced according to subtle changes in one of the former parameters under reaction conditions.

It is generally assumed that the distinct activity and selectivity for CO<sub>2</sub>RR of bimetallic alloy catalysts might be assigned to changes in their electronic and geometric structure originating from the modification of the interatomic distance of surface atoms brought about by the incorporation of a different atom in the lattice<sup>71,72</sup>. These changes lead to strain and altered binding strengths of reaction intermediates by shifting the center of the electronic d-band. Such effects have been demonstrated for Cu overlayers on Pt<sup>73</sup>, where the CH<sub>4</sub> production was found to increase with increasing film thickness under tensile strain. Core-shell bimetallic structures with an inexpensive core are also of interest for CO<sub>2</sub>RR, especially in cases where ultrathin Cu layers can be stabilized at the NP surface on other metals that would lead to expansive lattice strain, since under such conditions a more favorable stabilization of the reaction intermediates has been predicted<sup>74</sup>.

The reaction selectivity has also been shown to be strongly dependent on the composition of the bimetallic system. For example, for bimetallic AuCu NPs, Kim et al.<sup>75</sup> described increased CO production with increasing Au content, with the optimal Au<sub>3</sub>Cu composition leading to a mass activity exceeding 200 A g<sup>-1</sup> at  $-0.73$  V vs RHE. However, the distinct CO selectivity could not be exclusively assigned to changes in the electronic structure (Figure 3a), due to the similarities observed for pure Au and Au<sub>3</sub>Cu. Instead, synergetic electronic and geometric effects had to be invoked for the AuCu NPs in order to understand their altered activity for CO<sub>2</sub>RR through the modification of the intermediate binding strength (Figure 3b). Similar results were found by Li et al.<sup>70</sup> for mesoporous PdCu with Pd<sub>7</sub>Cu<sub>3</sub> exhibiting the highest activity for CO production with over 80% FE. Based on DFT calculations, Pd atoms were found to act as reactive centers and promote CO desorption by altering the electronic

structure of Cu at neighboring Pd sites, increasing thus the CO<sub>2</sub> to CO selectivity. Along these lines, distinct selectivity trends were reported for PdCu NPs with ordered, disordered, and phase-separated atomic arrangements (Figure 3c)<sup>68</sup>. In particular, phase-separated PdCu NPs exhibited high selectivity for C<sub>2</sub> products (>60% FE), while an ordered PdCu catalyst generated C<sub>1</sub> products (>80% FE). The degree of intra-particle atomic ordering was also shown to control the selectivity of AuCu NPs (Figure 3d)<sup>76</sup>, with disordered AuCu NPs favoring H<sub>2</sub> production while ordered AuCu NPs converted CO<sub>2</sub> to CO. These results highlight that the atomic ordering of the metal constituents in bimetallic catalysts plays an important role in determining the catalytic selectivity. Surface segregation of one of the bimetallic components under CO<sub>2</sub>RR reaction conditions should also be taken into consideration. For example, for small size-controlled AuCu catalysts, Au surface segregation was found to lead to an increase in CO selectivity at the expense of hydrocarbons<sup>22</sup>. Direct evidence of the surface segregation phenomena was also reported via quasi *in situ* XPS and *operando* XAS for CoCu catalysts, which revealed Cu surface segregation under reaction conditions (Figure 3d)<sup>74</sup>. Nevertheless, in both cases due to the small size of the NPs (below 5 nm) and the large number of undercoordinated surface sites and the compressive strain of the Cu lattice at the NP shell due to the Co core, CO and H<sub>2</sub> selectivity was favored instead of multicarbon products.

The use of co-catalysts has also been proposed as a possible viable alternative to enhance multicarbon product generation by contributing CO-producing sites that facilitate reaction pathways involving \*CO intermediates. One notable example is the work of Ren et al. on oxide-derived Cu-Zn catalysts<sup>77</sup> which demonstrated enhanced C<sub>2</sub>H<sub>5</sub>OH production (29% FE and -8.2 mA cm<sup>-2</sup> at -1.05 V vs RHE) for a Cu<sub>4</sub>Zn composition. *Operando* Raman spectroscopy data revealed adsorbed CO only on Cu sites, and it was postulated to originate from the spillover of CO from the Zn to the Cu site and deemed crucial for the formation of C<sub>2</sub>H<sub>5</sub>OH at the Cu surface (Figure 3e). Subsequently, the combined effects of CO spillover and atomic ordering were proposed by Lee et al. for phase-separated and phase-blended Ag-Cu<sub>2</sub>O electrodes<sup>78</sup>. Incorporating Ag into Cu<sub>2</sub>O was shown to result in higher C<sub>2</sub>H<sub>5</sub>OH production as compared to pure Cu<sub>2</sub>O, which was also assigned to an increase in CO population arising from the Ag sites. Moreover, the phase-blended Ag-Cu<sub>2</sub>O catalyst showed higher ethanol selectivity than phase-separated Ag-Cu<sub>2</sub>O, even though the Ag content on the surface of the phase-separated Ag-Cu<sub>2</sub>O electrode was reported to be larger. It was proposed that an optimum distribution and distance between the Ag and Cu atoms was important in order to facilitate efficient CO transfer from Ag to Cu sites, thus enhancing the product selectivity toward ethanol.

The reactivity of bimetallic catalysts for CO<sub>2</sub>RR is affected by a variety of factors that must be considered for their rational design. Based on the literature<sup>22,67-83</sup>, it seems that the modification of the intra-particle atomic arrangement and spillover effects must be considered in order to develop bimetallic catalysts for generating C<sub>2+</sub> products. However, it should also be noted that the majority of the previous studies are based on experimental data acquired on the as prepared samples, not considering that the

surface composition and chemical state of the catalyst may change during the reaction. Additional attention needs to be dedicated in the future to the implementation and use of *in situ* and *operando* techniques (e.g. XAFS, XPS, Liquid-TEM, etc.) to gain in depth information on the dynamic behavior of the structure and composition of CO<sub>2</sub>RR electrocatalysts.

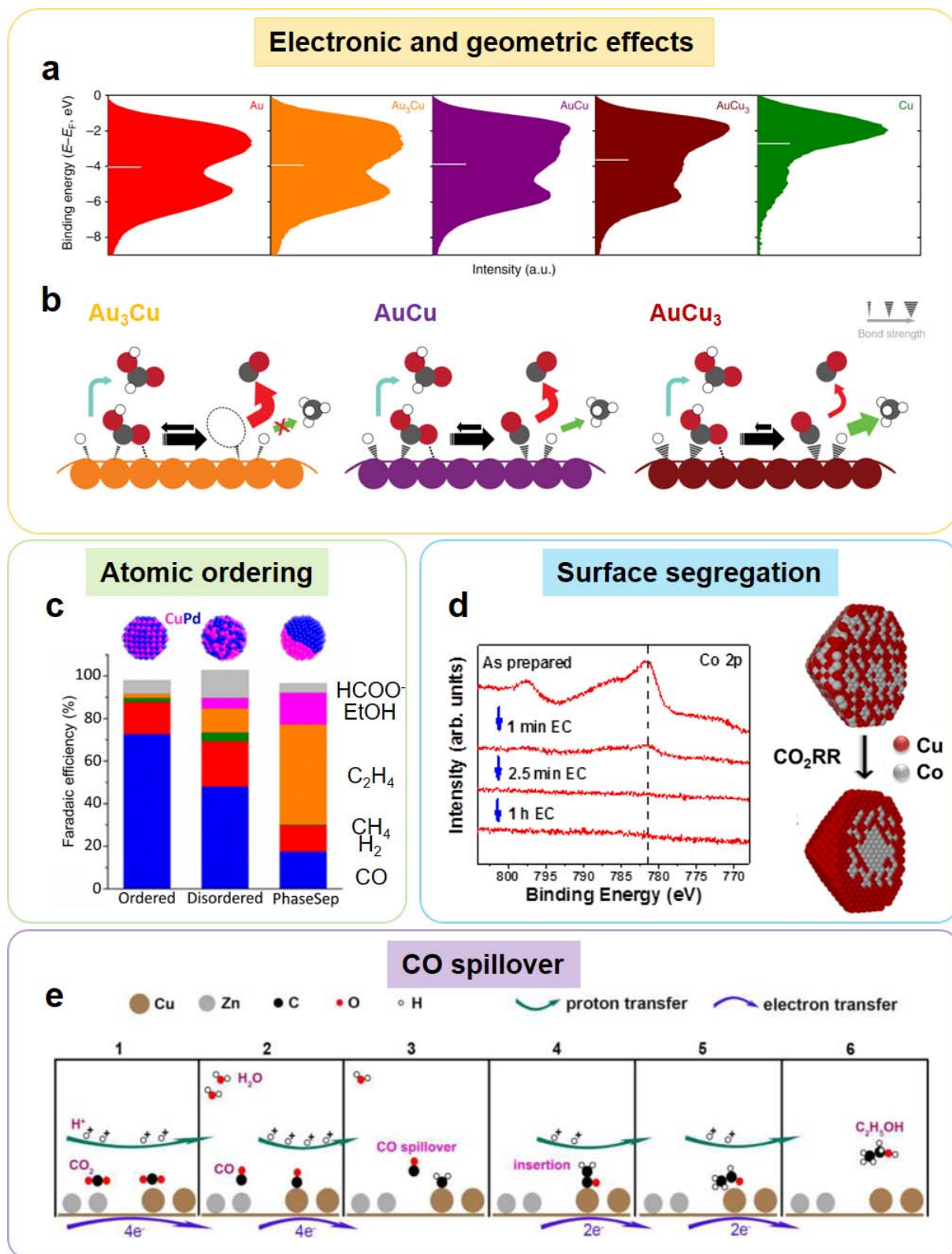


**Figure 3. Various parameters affecting the CO<sub>2</sub>RR selectivity of Cu-based bimetallic catalysts.** (a) Surface valence band photoemission spectra of AuCu bimetallic NPs. The white bar indicates the center of the d-band. (b) CO<sub>2</sub>RR mechanism for AuCu bimetallic NPs describing changes in the binding of reaction intermediates. (c) FEs of PdCu NPs with different mixing patterns. (d) Quasi *in situ* XPS spectra of the Co2p core level region of CoCu NPs as a function of various CO<sub>2</sub> electroreduction times at -1.1 V vs RHE. Model representation for surface segregation of CoCu NPs under CO<sub>2</sub>RR. (e) Proposed mechanism for CO<sub>2</sub>RR to C<sub>2</sub>H<sub>5</sub>OH on Cu<sub>x</sub>Zn catalysts. Figures adapted with permission from: **a,b** ref. <sup>75</sup>, Nature Publishing Group; **c** ref. <sup>68</sup>, American Chemical Society; **d** ref. <sup>74</sup>, Elsevier and **e** ref. <sup>77</sup>, American Chemical Society.

**Non-Cu catalysts.** A key descriptor that allows Cu to produce hydrocarbons and alcohols is having a moderate binding strength of the CO intermediate. Therefore, it might be possible to get a comparable CO binding strength by combining a metal that binds CO strongly with another that binds CO weakly. For example, a Pd-modified Au electrode was reported to be able to reduce CO<sub>2</sub> to C<sub>1</sub>-C<sub>5</sub> hydrocarbons<sup>84</sup>. This strategy was also applied to non-noble metals, such as NiGa<sup>85</sup> and NiAl<sup>86</sup>. However, these catalysts still showed very poor selectivity toward hydrocarbons<sup>84,85</sup> and alcohols<sup>86</sup> (<5% FE). In general, nanostructuring metal surfaces will induce the formation of defects and low-coordinated sites, which could bind CO stronger as compared to their bulk counterparts.<sup>87</sup> This significant change of the surface coordination might transform a CO-producing catalyst (weak CO binding) into a hydrocarbon/alcohol-producing catalyst. Nevertheless, it should also be considered that when the size of the electrocatalyst is further reduced, and very high populations of under-coordinated atoms are present, a stronger H-binding (competing HER) would result in a weakening of the CO binding and a switch in the selectivity from CO to H<sub>2</sub>, as was observed before for Au NPs<sup>21</sup> and Zn NPs<sup>23</sup> below 8 nm. Nonetheless, highly porous Ag foam catalysts demonstrated a ~60% FE toward methane and ethylene at -1.5 V vs RHE (Figure 4a)<sup>88</sup>. This remarkable Cu-like behavior was rationalized in terms of the significantly increased CO binding energy of the mesoporous Ag foam. This phenomenon, observed at very high overpotentials, might inspire researchers to re-think the catalytic performance of other highly defective nanostructured Ag catalysts which usually produce only CO at low overpotentials<sup>89</sup>. Furthermore, when the early transition metals, such as Mo, W, Ta, Fe, and Ti (strong CO binding), are converted to carbides, the binding energy of CO was found to become weaker due to a more carbophobic and oxophilic nature of these carbides<sup>90</sup>. For instance, Mo<sub>2</sub>C could reduce CO<sub>2</sub> to methane at lower overpotentials (-0.55 V ~ -0.8 V vs RHE) as compared to Cu, although with a very low efficiency (<0.1% FE)<sup>91</sup>. Transition metal chalcogenides have been theoretically predicted to be active for CO<sub>2</sub>RR<sup>92</sup>, and MoS<sub>2</sub> was reported to reduce CO<sub>2</sub> to n-propanol (~3.5% FE) in 0.1 M NaHCO<sub>3</sub><sup>93</sup>. However, the selectivity toward hydrocarbons and alcohols was severely suppressed due to the more favorable hydrogen evolution pathway on the carbide and chalcogenide catalysts in aqueous electrolytes. Recently, nickel phosphide

(Ni<sub>2</sub>P) was reported to selectively reduce CO<sub>2</sub> to C<sub>3</sub> and C<sub>4</sub> products at overpotentials as low as 10 mV (e.g., 71% FE for 2,3-furandiol at 0 V vs RHE), but the current density was quite low (<0.5 mA cm<sup>-2</sup>)<sup>94</sup>.

Theoretical predictions have indicated that single-atom catalysts with an active metal atom embedded either in another metal (nitride/carbide)<sup>95,96</sup> or in a nitrogen-doped carbon matrix<sup>97,98</sup> also have the potential to reduce CO<sub>2</sub> to higher products beyond CO and formate. Single-Ir-doped TiC (Ir@TiC) was found to have a remarkably low overpotential of -0.09 V to selectively produce methane<sup>95</sup>. Cheng et al.<sup>96</sup> theoretically studied a series of single-atom alloys with the majority component being either gold or silver in combination with isolated single atoms (Rh, Ir, Cu, Ni, Pd, Pt, and Co) replacing surface atoms and found Rh@Au(100) and Rh@Ag(100) to be the most active combinations for methane formation. Theoretical investigations of single transition metal atoms anchored on defective graphene with single (M@sv-Gr) or double vacancies (M@dv-Gr) revealed Ni@dv-Gr and Pt@dv-Gr as promising materials for methanol production and Os@dv-Gr and Ru@dv-Gr for methane production<sup>97</sup>. While these theoretical studies showed great potential, significant production of hydrocarbons or alcohols on realistic single atom catalysts still needs to be experimentally demonstrated. Recently, Ju et al.<sup>98</sup> reported high CO selectivity (85% FE) for metal- and nitrogen-doped porous carbons with porphyrin-like C-N structures (M-N-C, M = Mn, Fe, Co, Ni, Cu). In addition, Mn-N-C and Fe-N-C were also found to produced trace amounts of methane (<0.5% FE), which was assigned to the stronger CO binding of the Fe and Mn porphyrine-like structures<sup>99</sup>. The selective production of acetic acid (61% FE at -0.5 V vs Ag/AgCl) over ferrihydrite-like (Fh-FeOOH) clusters supported on N-doped carbon was also reported.<sup>100</sup> Here the reactivity was correlated to the formation of nitrogen-coordinated iron (II) sites as single atoms or polyatomic species at the interface between iron oxyhydroxide and the nitrogen-doped carbon, and to the N species acting concertedly to enable the C-C coupling.

The role of N or N-C species in C-C formation during CO<sub>2</sub>RR was further described in metal-free carbon materials<sup>101-105</sup>. N-doped graphene quantum dots (NGQDs) showed a ~55% FE for multicarbon products and partial current densities of 46 and 21 mA cm<sup>-2</sup> for ethylene and ethanol at -0.86 V vs RHE respectively, which is comparable to those obtained with Cu NPs catalysts (Figure 4b)<sup>101</sup>. The fact that GQDs primarily yielded CO and formate demonstrated the decisive role of the pyridinic N species at the utmost exposed edge sites of NGQDs in the C-C formation. Furthermore, N-doped nanodiamond showed a ~77% FE for acetic acid between -0.8 and -1.0 V vs RHE, resulting from its high hydrogen evolution potential and N-doping, where N-sp<sup>3</sup>C could be the most active species<sup>102</sup>. By further introducing boron, B- and N-co-doped diamond surprisingly reduced CO<sub>2</sub> to ethanol with 93.2% FE at -1.0 V vs RHE<sup>103</sup>, while the B-doped diamond mainly produced formaldehyde<sup>103,104</sup>. The high ethanol selectivity could be attributed to the synergetic effect of B and N co-doping and fine-balance between N content and hydrogen evolution potential. However, the reaction pathways regarding a variety of the major products from acetic acid, to formaldehyde and ethanol with the different dopant species still needs to be clarified by additional experimental work and theoretical calculations.

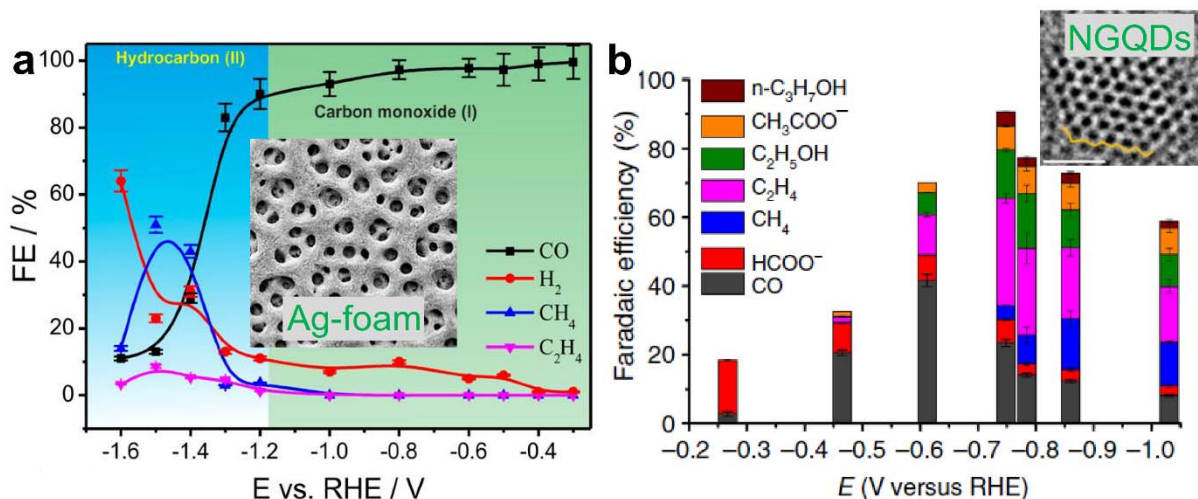


**Figure 4. Non-Cu catalysts for the production of hydrocarbons and oxygenates.** Potential-dependent FEs of CO<sub>2</sub>RR products over (a) an Ag foam catalyst and (b) N-doped graphene quantum dots (NGQDs). The insert in (a) displays a SEM image of the Ag-foam and that in (b) a TEM image of a single NGQD containing a zigzag edge (outlined by a yellow line). Figures adapted with permission from: **a** ref. <sup>88</sup>, American Chemical Society and **b** ref. <sup>101</sup>, Nature Publishing Group.

## Electrolyte design for C<sub>2+</sub> production

The role of the electrolyte cannot be neglected in an electrochemical reaction, since it will participate in the reaction through its interactions with electrode surface as well as the reactants, intermediates and products. Understanding these effects on the catalyst structure and the reactivity will help improve the CO<sub>2</sub>RR activity and C<sub>2+</sub> selectivity *via* rational electrolyte design.

**Electrolyte effect on catalyst structure.** It has been shown that CO<sub>2</sub>RR is a reaction strongly sensitive to the structure of the electrode and therefore, dynamic processes that such electrode might undergo upon exposure to the electrolyte and applied potential must be considered. Thorough spectroscopic and microscopy characterization, before, after, but even more importantly, under *operando* reaction conditions are key to understand the real nature of the catalytically active sites<sup>45,88,106</sup>. For instance, a polycrystalline Cu electrode surface was found via EC-STM to undergo a significant surface reconstruction during CO<sub>2</sub>RR in 0.1 M KHCO<sub>3</sub> from a polycrystalline surface to a well-known ethylene-selective Cu(100) surface orientation within 3 hours at -0.9 V vs SHE<sup>107</sup>. This transformation became faster in 0.1 M KOH and had a transition stage with Cu(111) as intermediate orientation (Figure 5a-c)<sup>108</sup>. Nevertheless, no information could be found in the former work regarding a possible change in the selectivity of these catalyst with reaction time. Recently, *operando* EC-AFM measurements revealed that carbon-supported Cu nanocubes lose their cubic shape and decrease in size during CO<sub>2</sub>RR in 0.1 M KHCO<sub>3</sub>, and the morphology change was found to correlate with time-dependent activity and selectivity changes (Figure 2b)<sup>45</sup>.

Plasma-oxidized Cu foil catalysts with excellent  $C_{2+}$  selectivity were found to form shaped CuI particles on the surface in  $I^-$ -containing electrolytes even at open circuit potential (OCP), and the morphology of the shaped particles could be tuned by introducing different cations ( $K^+$  versus  $Cs^+$ ) in the electrolyte (Figure 5d-f)<sup>61,62</sup>. Remarkably, the electrolyte pre-restructured catalyst surfaces underwent different changes during  $CO_2RR$ . The CuI crystals were reduced to form a highly porous surface in the KI-containing electrolyte, while in the CsI-containing electrolyte some smaller CuI particles survived during the reaction, which helped to stabilize  $Cu^+$  species that were found to facilitate C-C coupling<sup>59</sup>. The larger cations ( $Cs^+$  versus  $K^+$ ) contributed more favorably to the stabilization of the CuI species.

Inspired by the dynamic evolution of catalyst structures induced by the electrolyte and the applied potential, an electrolyte-driven nanostructuring strategy was applied to synthesize efficient  $CO_2RR$  catalysts. By cycling an electropolished Cu foil in a KCl solution, well-defined Cu nanocubes (Figure 5g)<sup>44</sup> could be grown on the surface with sizes that could be tuned by changing the KCl concentration. In combination with low-pressure  $O_2$  plasma pre-activation, these Cu nanocubes catalysts showed a vastly improved selectivity toward  $C_2-C_3$  (73% FE) hydrocarbons and alcohols<sup>44</sup>. This synthesis method ensured well-defined Cu(100) facets in the as prepared samples and also better morphological stability during  $CO_2RR$  as compared to related systems prepared by the metal ion battery cycling method<sup>109</sup> or *in situ* generated in a KCl-containing  $KHCO_3$  solution<sup>42</sup>. Other halide salts (KBr, KI) were also used to modify the Cu surface and showed high  $C_{2+}$  selectivity. Moreover, when a polycrystalline Cu foil was electrochemically oxidized in concentrated KOH by an anodization process,  $Cu(OH)_2$  nanowires (Figure 5i)<sup>110</sup> were grown on the surface, which were further reduced to a Cu catalyst with mixed oxidation states under reaction conditions. These examples show the rich possibilities for the design of new catalysts via electrolyte-driven nanostructuring.

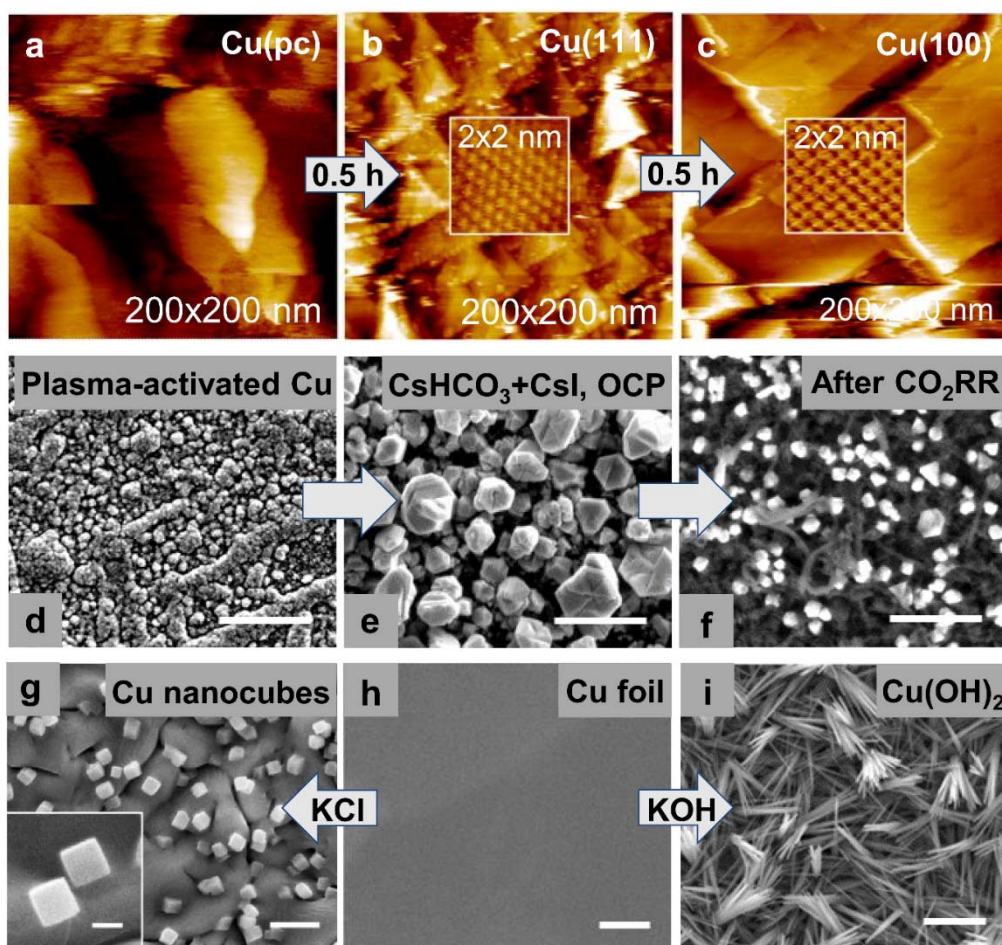


**Figure 5. Electrolyte effect on catalyst structure.** (a-c) EC-STM images of polycrystalline Cu acquired under CO<sub>2</sub>RR at  $-0.90$  V (vs SHE) in  $0.1$  M KOH after different reaction times. (d-f) SEM images displaying the surface morphology of an O<sub>2</sub>-plasma-oxidized Cu foil (d, left), and after immersion in CsHCO<sub>3</sub>+CsI at open circuit potential (OCP, e) and after 1 h of CO<sub>2</sub>RR at  $-1.0$  V vs RHE (f). All the scale bars are  $5$   $\mu$ m. (g-i) Electrolyte-driven nanostructuring of a pristine metallic Cu foil (h, scale bar:  $2$   $\mu$ m) and the same foil after cycling in KCl (g, scale bars:  $2$   $\mu$ m (image) and  $200$  nm (insert)) and in KOH (i, scale bar:  $5$   $\mu$ m). Figures adapted with permission from: **a-c** ref. <sup>108</sup>, Springer; **d** ref. <sup>61</sup>, American Chemical Society; **e,f**, ref. <sup>62</sup>, American Chemical Society; **g,h** ref. <sup>44</sup>, American Chemical Society and **i** ref. <sup>110</sup>, American Chemical Society.

**Electrolyte effect on CO<sub>2</sub>RR reactivity.** Apart from the obvious effect on the catalyst structure, electrolytes also play an important chemical role in the CO<sub>2</sub>RR. Understanding mechanistically the electrolyte effect would help improve the activity and selectivity of CO<sub>2</sub>RR via efficient electrolyte design. The size of alkali metal cations was shown to strongly affect the product distribution over Cu-based catalysts and the presence of larger cations (e.g., K, Cs) facilitated the formation of C<sub>2+</sub> products over both, metallic Cu<sup>111-113</sup> and CuO<sub>x</sub> catalysts (Figure 6a,b). The effect of alkali metal cations on the reaction pathways is still under debate. Singh et al.<sup>111</sup> theoretically interpreted the effect by preferential

cation hydrolysis in the vicinity of the electrode and proposed that the stronger buffering effect of larger cations lowered the local pH near the electrode, leading to higher local CO<sub>2</sub> concentration. This hypothesis was verified experimentally by probing the pH at the electrode-electrolyte interface using *in situ* surface-enhanced infrared absorption spectroscopy and *operando* Raman spectroscopy<sup>49,114</sup>. DFT calculations revealed that the intermediates toward C<sub>2+</sub> formation were stabilized by the electrostatic interactions between solvated cations at the outer Helmholtz plane (OHP) and adsorbed species having large dipole moments.<sup>112</sup> While cations only populated the OHP in these studies over metallic Cu surfaces<sup>96</sup>, a recent study from Gao et al.<sup>62</sup> revealed that the solvated cations can be specifically adsorbed on both metallic and pre-oxidized Cu electrode surfaces under CO<sub>2</sub>RR conditions when the explicit surface solvation around the adsorbed cation is considered. Following the same DFT-based modeling method, subsurface oxygen was found to promote the specific adsorption of cations and accentuated the effect of the cations, significantly promoting CO\* formation (one of the intermediates toward C<sub>2+</sub>), Figure 6c.<sup>62</sup> In addition to the alkali metal cations, the presence of multivalent cations can also accelerate CO<sub>2</sub>RR rate and influence the product selectivity. On a CuSnPb alloy electrode<sup>115</sup>, the CO<sub>2</sub>RR rate in a La<sup>3+</sup>-containing acidic electrolyte was two-times higher than that in Na<sup>+</sup> at the same potential, and in the presence of Zr<sup>4+</sup>, CH<sub>3</sub>CHO (17.6% FE) was produced, while CH<sub>3</sub>OH (35% FE) and HCOOH (28% FE) were produced in the presence of Na<sup>+</sup>. However, the application of multivalent cations was limited by their low solubility.

Aqueous solutions of bicarbonate salts, rather than other anions (e.g., SO<sub>4</sub><sup>2-</sup>, ClO<sub>4</sub><sup>-</sup>), are generally used as electrolyte for CO<sub>2</sub>RR since a higher effective CO<sub>2</sub> concentration near the electrode surface is accessible through a rapid equilibrium between bicarbonate and the dissolved CO<sub>2</sub> molecule, as observed by *operando* FTIR<sup>116-118</sup>. In combination with the presence of halides in the bicarbonate electrolyte, the formation of C<sub>2+</sub> products over plasma-oxidized Cu catalysts was significantly increased (Figure 6b)<sup>61,62</sup>, which was attributed to the specific adsorption of halides with a higher coverage on the pre-oxidized Cu surface during the reaction, (as shown in Figure 5b)<sup>61,62</sup>. However, in contrast to the metallic Cu foil, when a metallic Cu (100) single crystal electrode<sup>119</sup> was measured in pure potassium halide electrolytes, the formation of ethylene and ethanol increased from Cl<sup>-</sup> to Br<sup>-</sup> to I<sup>-</sup>. The specifically adsorbed halides could participate in the initial activation of CO<sub>2</sub> as well as the further hydrogenation through a strong interaction with the adsorbed intermediates<sup>61,62,119-121</sup>.

To minimize the competing HER, a higher electrolyte pH (the concentration of H<sup>+</sup> or OH<sup>-</sup>) is preferred. Meanwhile, higher (local) pH also favors the formation of ethylene over methane<sup>52,122</sup>. However due to the acidic nature of the CO<sub>2</sub> molecule, a strong alkaline electrolyte cannot be achieved in a regular H-type electrochemical cell<sup>18</sup>. The gas diffusion electrode configuration (GDE, Figure 6d)<sup>19</sup> used in a flow cell, with concentrated KOH instead of KHCO<sub>3</sub> as the electrolyte, makes the strong alkalinity possible, with the benefit of diffusion of CO<sub>2</sub> across the gas-liquid interface. By increasing the KOH concentration from 1 M to 10 M, ethylene started to evolve over a Cu GDE already at -0.165

V vs RHE almost simultaneously with the CO production (Figure 6e)<sup>19</sup>. Similarly, Jouny et al.<sup>123</sup> reported CO electroreduction over oxide-derived Cu catalysts in a flow cell with a C<sub>2+</sub> FE of 91% and 630 mA cm<sup>-2</sup> at -0.67 V vs RHE, which pushed closer the CO<sub>2</sub>RR to future industrial applications. However, the challenge remains regarding how to increase the commercially relevant long-term stability of catalysts in the GDE configuration while maintaining the initial high activity and C<sub>2+</sub> selectivity.

The finite CO<sub>2</sub> solubility in water (33 mM at 25 °C, 1 atm) leads to an upper, diffusion-limited CO<sub>2</sub>RR rate. While using the GDE configuration one could bypass this issue, increasing the CO<sub>2</sub> pressure (even supercritical conditions) would also increase the CO<sub>2</sub> concentration in aqueous electrolytes<sup>124,125</sup>. Nevertheless, more effort is still needed to address critical issues arising in the high pressure configuration such as the corrosion of the Cu electrodes and the formation of carbon deposits. Compared to water, some organic solvents (e.g., acetonitrile, methanol and N,N-dimethylformamide) and ionic liquids have several-fold higher CO<sub>2</sub> solubility and can be used as an alternative reaction media. In addition to being a solvent, an ionic liquid can also serve as a co-catalyst in the aqueous electrolyte due to its complexation ability with CO<sub>2</sub> which lowers the energy of the initial reduction barrier<sup>126</sup>. For example, a Cu(I)/C-doped boron nitride catalyst reduced CO<sub>2</sub> to acetic acid with 80.3% FE when 1-ethyl-3-methylimidazolium tetrafluoroborate ([Emim]BF<sub>4</sub>)-LiI-water solution was used as electrolyte<sup>127</sup>.

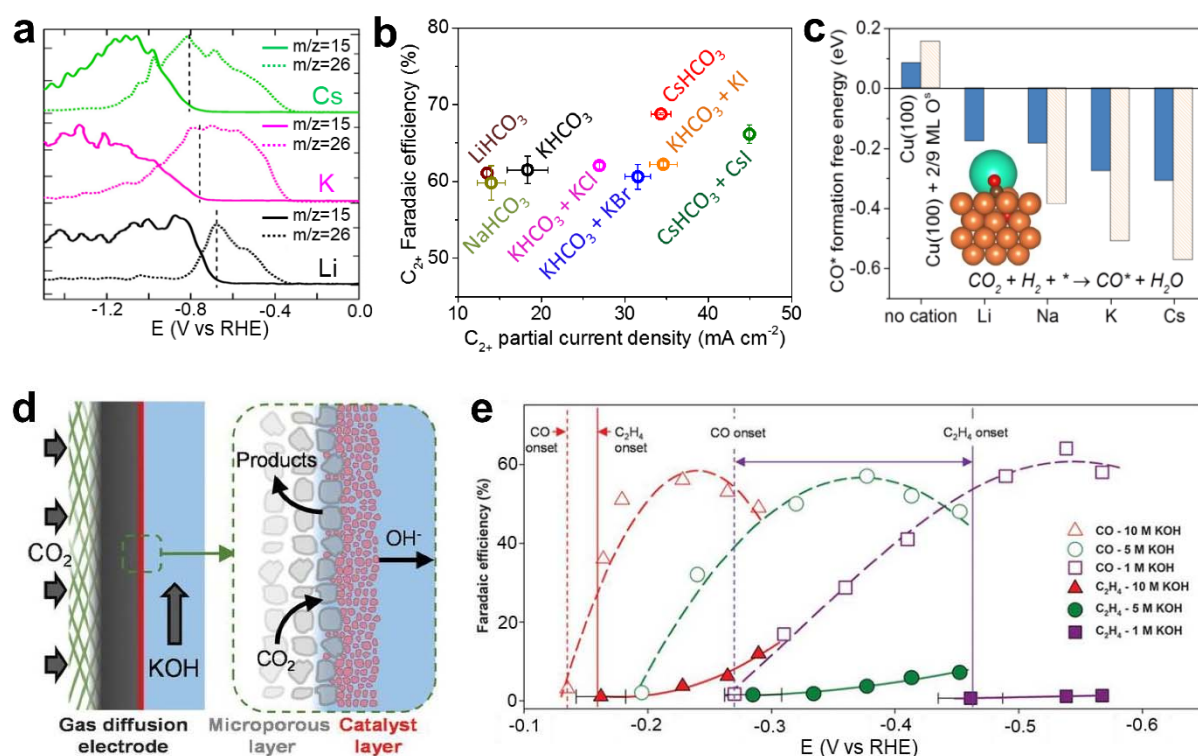


**Figure 6. Electrolyte effect on CO<sub>2</sub>RR reactivity.** (a) DEMS mass fragments associated with the reduction products formed during CO reduction on a Cu(100) electrode in different 0.1 M alkaline hydroxide solutions. (b) FEs and partial current densities of C<sub>2+</sub> products obtained from a plasma-oxidized Cu foil catalyst in different electrolytes after 1 h of CO<sub>2</sub>RR at -1.0 V vs RHE. (c) CO\* formation free energy for different cations. (d) Schematic of the GDE configuration. (e) Faradaic efficiency vs potential for CO and C<sub>2+</sub> products in different KOH concentrations.

formation free energy calculated in the absence and presence of Li\*, Na\*, K\*, and Cs\* on bare Cu(100) and Cu(100) with 2/9 ML subsurface oxygen (O<sup>s</sup>). (d) Schematic of the cathode portion of a gas diffusion electrode (GDE) for CO<sub>2</sub>RR. (e) C<sub>2</sub>H<sub>4</sub> and CO FEs of a Cu GDE in KOH with different concentrations. Figures adapted with permission from: **a** ref. <sup>113</sup>, American Chemical Society; **b** ref. <sup>61,62</sup>, American Chemical Society; **c** ref. <sup>62</sup>, American Chemical Society and **d,e** ref. <sup>19</sup>, American Association for the Advancement of Science.

## Summary and outlook

As discussed in the present review, the CO<sub>2</sub>RR over a real (complex) catalyst is controlled by multiple factors including surface roughness, defect density, nanoparticle size, shape, composition, interparticle distance, and the electrolyte<sup>13</sup>. To disentangle their relative contributions, further investigations on morphologically and chemically well-defined model catalysts are required. The fundamental knowledge that can be gained from the former systems can be used to create an optimum catalyst configuration leading to a given desired activity and selectivity. Furthermore, most of the current studies focusing on facilitating the C-C coupling were conducted on metallic Cu systems. Additional work on other relevant model materials including Cu alloys, segregated Cu-bimetallic systems as well as active non-Cu-based systems should be further developed.

The application of *in situ* and *operando* characterization techniques in CO<sub>2</sub>RR studies is highly desired, since we have learned that the insights from those characterization techniques do help the rational design of efficient catalysts and electrolytes. For example, we reported the positive correlation between ethylene formation and the presence of Cu<sup>+</sup> species based on an *operando* XAFS study<sup>57</sup> followed by the quasi *in situ* XPS work<sup>44,45</sup> correlating the selectivity for C<sub>2+</sub> products to the content of Cu<sup>+</sup> species stabilized on Cu nanocubes after O<sub>2</sub>-plasma pre-treatments as well as at Cu cube/Cu substrate interfaces. Later on the role of halides and cations in the electrolyte in the stability of Cu<sup>+</sup> (e.g. as CuI) and subsurface oxygen species<sup>61,62</sup> was also discussed, and a correlation found with the C<sub>2+</sub> selectivity. Such findings were later on used in the design of Cu catalysts by other groups<sup>60</sup>. These important advances clearly show the crucial role of *in situ* and *operando* techniques in electrocatalysis studies.

By rational design of catalytic electrodes and electrolytes, improved selectivity and C<sub>2+</sub> production rate from the CO<sub>2</sub>RR could be achieved. The use of a gas diffusion electrode configuration is already helping to close the gap between laboratory discovery and industrial needs, achieving by now already over 80% FE for C<sub>2+</sub> and >0.5 A cm<sup>-2</sup> partial current density at reasonable overpotentials<sup>19,123</sup>. However, the long-term stability of these catalysts at such high activity and selectivity still poses a significant challenge. Furthermore, the selectivity towards a specific C<sub>2+</sub> product (e.g., ethylene) should also be

improved to reduce the final cost due to product separation. In addition, new efforts should be made to develop a PEMFC-like electrochemical reactor fed only with humidified CO<sub>2</sub>, which could achieve liquid-electrolyte-free CO<sub>2</sub>RR, at least in the cathode side, as reported in a few cases<sup>24,25</sup>, promoting the formation of hydrocarbons and completely avoiding issues related to the low solubility of CO<sub>2</sub> in water.

Numerous reports have correlated CO<sub>2</sub>RR reactivity trends to specific catalyst structure/electrolyte configurations, highlighting the role played by the catalyst morphology, including its size, shape, defect density, composition, oxidation state as well as the chemical effect of electrolytes. Various possibilities have been theoretically proposed as plausible reaction pathways and active sites for each specific product of interest, although experimental verification under *operando* reaction conditions is still needed. Unfortunately, many calculations still only consider the thermodynamically free energy of reactants/intermediate/products, neglecting the effect of the electrolyte and the applied field. To understand electrified solid/liquid and solid/liquid/gas interfaces in electrochemical reactions, better theoretical models are needed that include the effect of the potential and the electrolyte<sup>128</sup>. For example, a proper surface solvation model of the electrolyte-electrode interface determines whether alkali metal cations can be adsorbed on metal surfaces under CO<sub>2</sub>RR conditions<sup>62,129</sup>.

More importantly, the identification of active sites strongly relies on the precision of the characterization techniques employed, which is actually heavily restricted under the usual complex electrochemical conditions. The possible changes in oxidation state, structure and even morphology of the catalysts in air after a given CO<sub>2</sub> treatment make difficult to identify active sites from experimental results collected *ex situ* before and after the reaction.

Therefore, serious efforts are already being made and more will need to be made in the years to come to further develop *operando* characterization techniques compatible with a liquid environment under CO<sub>2</sub>RR conditions, including the flow cell electrolyzer configurations that could effectively address the mass transport issues in the current *in situ* cells<sup>16,17</sup>. Furthermore, there is an urgent need to improve signal intensities of some *in situ* and *operando* scattering and spectroscopy techniques due to the low coverages of key reaction intermediates. Promising methods include XAS<sup>26,57</sup>, XPS<sup>44,45,74</sup>, FTIR<sup>10,116</sup>, Raman<sup>49,55,130,131</sup>, DEMS<sup>11,113</sup>, EC-AFM/STM<sup>45,108</sup> and Liquid-TEM<sup>132</sup>. With a synergistic combination of these tools, the identification of active sites and key reaction intermediates for the distinct reaction pathways that might be preferred under different electrode/electrolyte combinations will be possible. A closer interaction between experimental and theoretical groups in this field is also highly desirable, since it could serve to validate some of the new theoretical approaches that are currently being proposed to address the complexity of real CO<sub>2</sub>RR catalysts and electrolytes<sup>62,128</sup>. Furthermore, it will provide predictive guidance to the experimentalists searching for optimized material structures and compositions and the most favorable electrolytes.

## Acknowledgments

This work was supported by the European Research Council under grant ERC-OPERANDOCAT (ERC-725915) and the German Federal Ministry of Education and Research (BMBF) under grants #03SF0523C-‘CO2EKAT’ and #033RCOO4D-‘e-Ethylene’, as well as the Collaborative Research Centre (SFB) under grant #1316-‘Transient atmospheric plasmas - from plasmas to liquids to solids’.

## Competing interests

The authors declare no competing interests.

## References

1. Montoya, J. H. *et al.* Materials for solar fuels and chemicals. *Nat. Mater.* **16**, 70–81 (2017).
2. Haas, T., Krause, R., Weber, R., Demler, M. & Schmid, G. Technical photosynthesis involving CO<sub>2</sub> electrolysis and fermentation. *Nat. Catal.* **1**, 32–39 (2018).
3. Nielsen, D. U., Hu, X.-M., Daasbjerg, K. & Skrydstrup, T. Chemically and electrochemically catalysed conversion of CO<sub>2</sub> to CO with follow-up utilization to value-added chemicals. *Nat. Catal.* **1**, 244–254 (2018).
4. Whipple, D. T. & Kenis, P. J. A. Prospects of CO<sub>2</sub> Utilization via Direct Heterogeneous Electrochemical Reduction. *J. Phys. Chem. Lett.* **1**, 3451–3458 (2010).
5. Gao, D., Cai, F., Wang, G. & Bao, X. Nanostructured heterogeneous catalysts for electrochemical reduction of CO<sub>2</sub>. *Curr. Opin. Green Sustain. Chem.* **3**, 39–44 (2017).
6. Kortlever, R., Shen, J., Schouten, K. J. P., Calle-Vallejo, F. & Koper, M. T. M. Catalysts and Reaction Pathways for the Electrochemical Reduction of Carbon Dioxide. *J. Phys. Chem. Lett.* **6**, 4073–4082 (2015).
7. Lum, Y. & Ager, J. W. Evidence for product specific sites on oxide-derived Cu catalysts for electrochemical CO<sub>2</sub> reduction. *Nat. Catal.* (2019). doi:10.1038/s41929-018-0201-7
8. Montoya, J. H., Shi, C., Chan, K. & Nørskov, J. K. Theoretical Insights into a CO Dimerization Mechanism in CO<sub>2</sub> Electroreduction. *J. Phys. Chem. Lett.* **6**, 2032–2037 (2015).
9. Schouten, K. J. P., Qin, Z., Gallent, E. P. & Koper, M. T. M. Two pathways for the formation of ethylene in CO reduction on single-crystal copper electrodes. *J. Am. Chem. Soc.* **134**, 9864–9867 (2012).
10. Perez-Gallent, E., Figueiredo, M. C., Calle-Vallejo, F. & Koper, M. T. M. Spectroscopic Observation of a Hydrogenated CO Dimer Intermediate During CO Reduction on Cu(100) Electrodes. *Angew. Chemie - Int. Ed.* **56**, 3621–3624 (2017). **The first spectroscopic observation of a hydrogenated CO dimer Intermediate (\*OCCOH) on Cu(100) during CO Reduction using operando IR spectroscopy.**
11. Clark, E. L. & Bell, A. T. Direct Observation of the Local Reaction Environment during the Electrochemical Reduction of CO<sub>2</sub>. *J. Am. Chem. Soc.* **140**, 7012–7020 (2018).

12. Bertheussen, E. *et al.* Acetaldehyde as an Intermediate in the Electroreduction of Carbon Monoxide to Ethanol on Oxide-Derived Copper. *Angew. Chemie - Int. Ed.* **55**, 1450–1454 (2016).
13. Arán-Ais, R. M., Gao, D. & Roldan Cuenya, B. Structure- and Electrolyte-Sensitivity in CO<sub>2</sub> Electroreduction. *Acc. Chem. Res.* **51**, 2906–2917 (2018).
14. Larrazábal, G. O., Martín, A. J. & Pérez-Ramírez, J. Building Blocks for High Performance in Electrocatalytic CO<sub>2</sub> Reduction: Materials, Optimization Strategies, and Device Engineering. *J. Phys. Chem. Lett.* **8**, 3933–3944 (2017).
15. Zhu, D. D., Liu, J. L. & Qiao, S. Z. Recent Advances in Inorganic Heterogeneous Electrocatalysts for Reduction of Carbon Dioxide. *Adv. Mater.* **28**, 3423–3452 (2016).
16. Handoko, A. D., Wei, F., Jenndy, Yeo, B. S. & Seh, Z. W. Understanding heterogeneous electrocatalytic carbon dioxide reduction through operando techniques. *Nat. Catal.* **1**, 922–934 (2018).
17. Choi, Y. W., Mistry, H. & Roldan Cuenya, B. New insights into working nanostructured electrocatalysts through operando spectroscopy and microscopy. *Current Opinion in Electrochemistry* **1**, 95–103 (2017).
18. Weekes, D. M., Salvatore, D. A., Reyes, A., Huang, A. & Berlinguette, C. P. Electrolytic CO<sub>2</sub> Reduction in a Flow Cell. *Acc. Chem. Res.* **51**, 910–918 (2018).
19. Dinh, C. T. *et al.* CO<sub>2</sub> electroreduction to ethylene via hydroxide-mediated copper catalysis at an abrupt interface. *Science* **360**, 783–787 (2018). **Ethylene was selectively produced with 70% FE at –0.55 V vs RHE in a flow cell with GDE configuration and highly alkaline electrolyte.**
20. Reske, R., Mistry, H., Behafarid, F., Roldan Cuenya, B. & Strasser, P. Particle size effects in the catalytic electroreduction of CO<sub>2</sub> on Cu nanoparticles. *J. Am. Chem. Soc.* **136**, 6978–6986 (2014).
21. Mistry, H. *et al.* Exceptional Size-Dependent Activity Enhancement in the Electroreduction of CO<sub>2</sub> over Au Nanoparticles. *J. Am. Chem. Soc.* **136**, 16473–16476 (2014).
22. Mistry, H., Reske, R., Strasser, P. & Roldan Cuenya, B. Size-dependent reactivity of gold-copper bimetallic nanoparticles during CO<sub>2</sub> electroreduction. *Catal. Today* **288**, 30–36 (2017).
23. Jeon, H. S. *et al.* Operando Evolution of the Structure and Oxidation State of Size-Controlled Zn Nanoparticles during CO<sub>2</sub> Electroreduction. *J. Am. Chem. Soc.* **140**, 9383–9386 (2018).
24. Irabien, I. M.-G. and J. A. and A. Tailoring gas-phase CO<sub>2</sub> electroreduction selectivity to hydrocarbons at Cu nanoparticles. *Nanotechnology* **29**, 14001 (2018).
25. Ampelli, C. *et al.* Electrocatalytic conversion of CO<sub>2</sub> to produce solar fuels in electrolyte or electrolyte-less configurations of PEC cells. *Faraday Discuss.* **183**, 125–145 (2015).
26. Roth, C. *et al.* Determination of O[H] and CO coverage and adsorption sites on PtRu electrodes in an operating PEM fuel cell. *J. Am. Chem. Soc.* **127**, 14607–14615 (2005).
27. Velasco-Vélez, J.-J. *et al.* The role of the copper oxidation state in the electrocatalytic reduction of CO<sub>2</sub> into valuable hydrocarbons. *ACS Sustain. Chem. Eng.* (2018). doi:10.1021/acssuschemeng.8b05106
28. Saveleva, V. A. *et al.* Operando Evidence for a Universal Oxygen Evolution Mechanism on Thermal and Electrochemical Iridium Oxides. *J. Phys. Chem. Lett.* **9**, 3154–3160 (2018).
29. Wiltshire, R. J. K. *et al.* A PEM fuel cell for in situ XAS studies. in *Electrochimica Acta* **50**, 5208-5217 (2005).

30. Mistry, H. *et al.* Tuning Catalytic Selectivity at the Mesoscale via Interparticle Interactions. *ACS Catal.* **6**, 1075–1080 (2016).
31. Kim, D., Kley, C. S., Li, Y. & Yang, P. Copper nanoparticle ensembles for selective electroreduction of CO<sub>2</sub> to C<sub>2</sub>–C<sub>3</sub> products. *Proc. Natl. Acad. Sci.* **114**, 10560–10565 (2017).
32. Wang, X., Varela, A. S., Bergmann, A., Kühl, S. & Strasser, P. Catalyst Particle Density Controls Hydrocarbon Product Selectivity in CO<sub>2</sub> Electroreduction on CuOx. *ChemSusChem* **10**, 4642–4649 (2017).
33. Hori, Y., Takahashi, I., Koga, O. & Hoshi, N. Selective Formation of C<sub>2</sub> Compounds from Electrochemical Reduction of CO<sub>2</sub> at a Series of Copper Single Crystal Electrodes. *J. Phys. Chem. B* **106**, 15–17 (2002).
34. Huang, Y., Handoko, A. D., Hirunsit, P. & Yeo, B. S. Electrochemical Reduction of CO<sub>2</sub> Using Copper Single-Crystal Surfaces: Effects of CO Coverage on the Selective Formation of Ethylene. *ACS Catal.* **7**, 1749–1756 (2017).
35. Durand, W. J., Peterson, A. A., Studt, F., Abild-Pedersen, F. & Nørskov, J. K. Structure effects on the energetics of the electrochemical reduction of CO<sub>2</sub> by copper surfaces. *Surf. Sci.* **605**, 1354–1359 (2011).
36. Hahn, C. *et al.* Engineering Cu surfaces for the electrocatalytic conversion of CO<sub>2</sub>: Controlling selectivity toward oxygenates and hydrocarbons. *Proc. Natl. Acad. Sci.* **114**, 5918–5923 (2017).
37. Peterson, A. A., Abild-Pedersen, F., Studt, F., Rossmeisl, J. & Nørskov, J. K. How copper catalyzes the electroreduction of CO<sub>2</sub> into hydrocarbon fuels. *Energy Environ. Sci.* **3**, 1311 (2010).
38. Calle-Vallejo, F. & Koper, M. T. M. Theoretical considerations on the electroreduction of CO to C<sub>2</sub> Species on Cu(100) electrodes. *Angew. Chemie - Int. Ed.* **52**, 7282–7285 (2013).
39. Kim, Y. G., Javier, A., Baricuatro, J. H. & Soriaga, M. P. Regulating the Product Distribution of CO Reduction by the Atomic-Level Structural Modification of the Cu Electrode Surface. *Electrocatalysis* **7**, 391–399 (2016).
40. Schouten, K. J. P., Pérez Gallent, E. & Koper, M. T. M. Structure sensitivity of the electrochemical reduction of carbon monoxide on copper single crystals. *ACS Catal.* **3**, 1292–1295 (2013).
41. Chen, C. S. *et al.* Stable and selective electrochemical reduction of carbon dioxide to ethylene on copper mesocrystals. *Catal. Sci. Technol.* **5**, 161–168 (2015).
42. Roberts, F. S., Kuhl, K. P. & Nilsson, A. High selectivity for ethylene from CO<sub>2</sub> reduction over copper nanocube electrocatalysts. *Angew. Chemie - Int. Ed.* **54**, 5179–5182 (2015).
43. Loiudice, A. *et al.* Tailoring Copper Nanocrystals towards C<sub>2</sub> Products in Electrochemical CO<sub>2</sub> Reduction. *Angew. Chemie - Int. Ed.* **55**, 5789–5792 (2016).
44. Gao, D. *et al.* Plasma-Activated Copper Nanocube Catalysts for Efficient Carbon Dioxide Electroreduction to Hydrocarbons and Alcohols. *ACS Nano* **11**, 4825–4831 (2017).
45. Grosse, P. *et al.* Dynamic Changes in the Structure, Chemical State and Catalytic Selectivity of Cu Nanocubes during CO<sub>2</sub> Electroreduction: Size and Support Effects. *Angew. Chemie Int. Ed.* **57**, 6192–6197 (2018). **Dynamic changes of morphological and chemical states of Cu nanocubes during CO<sub>2</sub>RR were monitored using operando EC-AFM and EXAFS and correlated to the activity and selectivity.**
46. Dutta, A., Rahaman, M., Luedi, N. C., Mohos, M. & Broekmann, P. Morphology Matters:

- Tuning the Product Distribution of CO<sub>2</sub> Electroreduction on Oxide-Derived Cu Foam Catalysts. *ACS Catal.* **6**, 3804–3814 (2016).
47. Dutta, A., Rahaman, M., Mohos, M., Zanetti, A. & Broekmann, P. Electrochemical CO<sub>2</sub> Conversion Using Skeleton (Sponge) Type of Cu Catalysts. *ACS Catal.* **7**, 5431–5437 (2017).
  48. Reller, C. *et al.* Selective Electroreduction of CO<sub>2</sub> toward Ethylene on Nano Dendritic Copper Catalysts at High Current Density. *Adv. Energy Mater.* **7**, 1602114 (2017).
  49. Klingan, K. *et al.* Reactivity Determinants in Electrodeposited Cu Foams for Electrochemical CO<sub>2</sub> Reduction. *ChemSusChem* **11**, 3449–3459 (2018).
  50. Jeon, H. S., Kunze, S., Scholten, F. & Roldan Cuenya, B. Prism-Shaped Cu Nanocatalysts for Electrochemical CO<sub>2</sub> Reduction to Ethylene. *ACS Catal.* **8**, 531–535 (2018).
  51. Mariano, R. G., McKelvey, K., White, H. S. & Kanan, M. W. Selective increase in CO<sub>2</sub> electroreduction activity at grain-boundary surface terminations. *Science* **358**, 1187–1192 (2017).
  52. Tang, W. *et al.* The importance of surface morphology in controlling the selectivity of polycrystalline copper for CO<sub>2</sub> electroreduction. *Phys. Chem. Chem. Phys.* **14**, 76–81 (2012).
  53. Gupta, N., Gattrell, M. & MacDougall, B. Calculation for the cathode surface concentrations in the electrochemical reduction of CO<sub>2</sub> in KHCO<sub>3</sub> solutions. *J. Appl. Electrochem.* **36**, 161–172 (2006).
  54. Pander, J. E. *et al.* Understanding the Heterogeneous Electrocatalytic Reduction of CO<sub>2</sub> on Oxide-Derived Catalysts. *ChemElectroChem* **5**, 219–237 (2018).
  55. Mandal, L. *et al.* Investigating the Role of Copper Oxide in Electrochemical CO<sub>2</sub> Reduction in Real Time. *ACS Appl. Mater. Interfaces* **10**, 8574–8584 (2018).
  56. Lum, Y. & Ager, J. W. Stability of Residual Oxides in Oxide-Derived Copper Catalysts for Electrochemical CO<sub>2</sub> Reduction Investigated with <sup>18</sup>O Labeling. *Angew. Chemie - Int. Ed.* **57**, 551–554 (2018).
  57. Mistry, H. *et al.* Highly selective plasma-activated copper catalysts for CO<sub>2</sub> reduction to ethylene. *Nat. Commun.* **7**, 12123 (2016).
  58. Favaro, M. *et al.* Subsurface oxide plays a critical role in CO<sub>2</sub> activation by Cu(111) surfaces to form chemisorbed CO<sub>2</sub>, the first step in reduction of CO<sub>2</sub>. *Proc. Natl. Acad. Sci.* **114**, 6706–6711 (2017).
  59. Xiao, H., Goddard, W., Cheng, T. & Liu, Y. Cu metal embedded in oxidized matrix catalyst to promote CO<sub>2</sub> activation and CO dimerization for electrochemical reduction of CO<sub>2</sub>. *Proc. Natl. Acad. Sci.* **114**, 6685–6688 (2017). **The interface between Cu<sup>+</sup> and Cu<sup>0</sup> species improves significantly the kinetics and thermodynamics of both CO<sub>2</sub> activation and CO dimerization.**
  60. Zhou, Y. *et al.* Dopant-induced electron localization drives CO<sub>2</sub> reduction to C<sub>2</sub> hydrocarbons. *Nat. Chem.* **10**, 947–980 (2018).
  61. Gao, D., Scholten, F. & Roldan Cuenya, B. Improved CO<sub>2</sub> Electroreduction Performance on Plasma-Activated Cu Catalysts via Electrolyte Design: Halide Effect. *ACS Catal.* **7**, 5112–5120 (2017).
  62. Gao, D. *et al.* Activity and Selectivity Control in CO<sub>2</sub> Electroreduction to Multicarbon Products over CuO<sub>x</sub> Catalysts via Electrolyte Design. *ACS Catal.* **8**, 10012–10020 (2018). **By combining experiment and DFT calculations, a synergistic effect of the electrolyte (larger cations, halides) and the presence of subsurface oxygen species was found to stabilize Cu<sup>+</sup> species during CO<sub>2</sub>RR and improve the C<sub>2+</sub> production and stability of CuO<sub>x</sub> catalysts.**

63. Wang, L. *et al.* Electrochemical Carbon Monoxide Reduction on Polycrystalline Copper: Effects of Potential, Pressure, and pH on Selectivity toward Multicarbon and Oxygenated Products. *ACS Catal.* **8**, 7445–7454 (2018).
64. Clark, E. L. *et al.* Standards and Protocols for Data Acquisition and Reporting for Studies of the Electrochemical Reduction of Carbon Dioxide. *ACS Catal.* **8**, 6560–6570 (2018).
65. Schlögl, R. Heterogeneous catalysis. *Angew. Chemie - Int. Ed.* **54**, 3465–3520 (2015).
66. Garza, A. J., Bell, A. T. & Head-Gordon, M. Is Subsurface Oxygen Necessary for the Electrochemical Reduction of CO<sub>2</sub> on Copper? *J. Phys. Chem. Lett.* **9**, 601–606 (2018).
67. Yin, Z. *et al.* Highly selective palladium-copper bimetallic electrocatalysts for the electrochemical reduction of CO<sub>2</sub> to CO. *Nano Energy* **27**, 35–43 (2016).
68. Ma, S. *et al.* Electroreduction of CO<sub>2</sub> to hydrocarbons using bimetallic Cu-Pd catalysts with different mixing patterns. *J. Am. Chem. Soc.* **139**, 47–50 (2017). **Phase-separated CuPd bimetallic NPs achieved higher selectivity (>60%) for C<sub>2</sub> chemicals than ordered and disordered ones. Geometric effects rather than electronic effects seem to be key in determining the selectivity of bimetallic CuPd catalysts.**
69. Chen, D. *et al.* Tailoring the Selectivity of Bimetallic Copper–Palladium Nanoalloys for Electrocatalytic Reduction of CO<sub>2</sub> to CO. *ACS Appl. Energy Mater.* **1**, 883–890 (2018).
70. Li, M. *et al.* Mesoporous palladium-copper bimetallic electrodes for selective electrocatalytic reduction of aqueous CO<sub>2</sub> to CO. *J. Mater. Chem. A* **4**, 4776–4782 (2016).
71. Mavrikakis, M., Hammer, B. & Nørskov, J. K. Effect of strain on the reactivity of metal surfaces. *Phys. Rev. Lett.* **81**, 2819–2822 (1998).
72. Bligaard, T. & Nørskov, J. K. Ligand effects in heterogeneous catalysis and electrochemistry. *Electrochim. Acta* **52**, 5512–5516 (2007).
73. Reske, R. *et al.* Controlling catalytic selectivities during CO<sub>2</sub> electroreduction on thin Cu metal overlayers. *J. Phys. Chem. Lett.* **4**, 2410–2413 (2013).
74. Bernal, M. *et al.* CO<sub>2</sub> Electroreduction on Copper-Cobalt Nanoparticles: Size and Composition Effect. *Nano Energy* **53**, 27–36 (2018).
75. Kim, D., Resasco, J., Yu, Y., Asiri, A. M. & Yang, P. Synergistic geometric and electronic effects for electrochemical reduction of carbon dioxide using gold-copper bimetallic nanoparticles. *Nat Commun* **5**, 4948 (2014).
76. Kim, D. *et al.* Electrochemical Activation of CO<sub>2</sub> through Atomic Ordering Transformations of AuCu Nanoparticles. *J. Am. Chem. Soc.* **139**, 8329–8336 (2017).
77. Ren, D., Ang, B. S. H. & Yeo, B. S. Tuning the Selectivity of Carbon Dioxide Electroreduction toward Ethanol on Oxide-Derived Cu<sub>x</sub>Zn Catalysts. *ACS Catal.* **6**, 8239–8247 (2016). **CO spillover effect was observed and applied to facilitate selective CO<sub>2</sub>RR to ethanol on oxide-derived Cu<sub>x</sub>Zn catalysts.**
78. Lee, S., Park, G. & Lee, J. Importance of Ag-Cu Biphase Boundaries for Selective Electrochemical Reduction of CO<sub>2</sub> to Ethanol. *ACS Catal.* **7**, 8594–8604 (2017).
79. Clark, E. L., Hahn, C., Jaramillo, T. F. & Bell, A. T. Electrochemical CO<sub>2</sub> Reduction over Compressively Strained CuAg Surface Alloys with Enhanced Multi-Carbon Oxygenate Selectivity. *J. Am. Chem. Soc.* **139**, 15848–15857 (2017).
80. He, J., Johnson, N. J. J., Huang, A. & Berlinguette, C. P. Electrocatalytic Alloys for CO<sub>2</sub>

- Reduction. *ChemSusChem* **11**, 48–57 (2018).
81. Lum, Y. & Ager, J. W. Sequential catalysis controls selectivity in electrochemical CO<sub>2</sub> reduction on Cu. *Energy Environ. Sci.* **11**, 2935–2944 (2018).
  82. Carlos G. Morales-Guio Etosha R. Cave, Stephanie A. Nitopi, Jeremy T. Feaster, Lei Wang, Kendra P. Kuhl, Ariel Jackson, Natalie C. Johnson, David N. Abram, Toru Hatsukade, Christopher Hahn, T. F. J. Improved CO<sub>2</sub> reduction activity towards C<sub>2+</sub> alcohols on a tandem gold on copper electrocatalyst. *Nat. Catal.* **1**, 764–771 (2018).
  83. Jovanov, Z. P. *et al.* Opportunities and challenges in the electrocatalysis of CO<sub>2</sub> and CO reduction using bifunctional surfaces: A theoretical and experimental study of Au–Cd alloys. *J. Catal.* **343**, 215–231 (2016).
  84. Kortlever, R. *et al.* Palladium-gold catalyst for the electrochemical reduction of CO<sub>2</sub> to C<sub>1</sub>–C<sub>5</sub> hydrocarbons. *Chem. Commun.* **52**, 10229–10232 (2016).
  85. Torelli, D. A. *et al.* Nickel-Gallium-Catalyzed Electrochemical Reduction of CO<sub>2</sub> to Highly Reduced Products at Low Overpotentials. *ACS Catal.* **6**, 2100–2104 (2016).
  86. Paris, A. R. & Bocarsly, A. B. Ni-Al films on glassy carbon electrodes generate an array of oxygenated organics from CO<sub>2</sub>. *ACS Catal.* **7**, 6815–6820 (2017).
  87. Verdaguer-Casadevall, A. *et al.* Probing the Active Surface Sites for CO Reduction on Oxide-Derived Copper Electrocatalysts. *J. Am. Chem. Soc.* **137**, 9808–9811 (2015).
  88. Dutta, A., Morstein, C. E., Rahaman, M., Cedeño López, A. & Broekmann, P. Beyond Copper in CO<sub>2</sub> Electrolysis: Effective Hydrocarbon Production on Silver Nano-Foam Catalysts. *ACS Catal.* **8**, 8357–8368 (2018). **By creating high density of defects and lower-coordinated sites, one could transform a CO-producing catalyst (with weak CO binding) into a hydrocarbon- and alcohol-producing catalyst.**
  89. Mistry, H. *et al.* Enhanced CO<sub>2</sub> Electroreduction to CO over Defect-Rich Plasma-Activated Silver Catalysts. *Angew. Chemie Int. Ed.* **56**, 11394–11398 (2017).
  90. Michalsky, R., Zhang, Y. J., Medford, A. J. & Peterson, A. A. Departures from the adsorption energy scaling relations for metal carbide catalysts. *J. Phys. Chem. C* **118**, 13026–13034 (2014).
  91. Kim, S. K., Zhang, Y. J., Bergstrom, H., Michalsky, R. & Peterson, A. Understanding the Low-Overpotential Production of CH<sub>4</sub> from CO<sub>2</sub> on Mo<sub>2</sub>C Catalysts. *ACS Catal.* **6**, 2003–2013 (2016).
  92. Chan, K., Tsai, C., Hansen, H. A. & Nørskov, J. K. Molybdenum sulfides and selenides as possible electrocatalysts for CO<sub>2</sub> reduction. *ChemCatChem* **6**, 1899–1905 (2014).
  93. Francis, S. A. *et al.* Reduction of aqueous CO<sub>2</sub> to 1-Propanol at MoS<sub>2</sub> electrodes. *Chem. Mater.* **30**, 4902–4908 (2018).
  94. Calvino, K. U. D. *et al.* Selective CO<sub>2</sub> reduction to C<sub>3</sub> and C<sub>4</sub> oxyhydrocarbons on nickel phosphides at overpotentials as low as 10 mV. *Energy Environ. Sci.* **11**, 2550–2559 (2018).
  95. Back, S. & Jung, Y. TiC- and TiN-Supported Single-Atom Catalysts for Dramatic Improvements in CO<sub>2</sub> Electrochemical Reduction to CH<sub>4</sub>. *ACS Energy Lett.* **2**, 969–975 (2017).
  96. Cheng, M. J., Clark, E. L., Pham, H. H., Bell, A. T. & Head-Gordon, M. Quantum Mechanical Screening of Single-Atom Bimetallic Alloys for the Selective Reduction of CO<sub>2</sub> to C<sub>1</sub> Hydrocarbons. *ACS Catal.* **6**, 7769–7777 (2016).
  97. Back, S., Lim, J., Kim, N. Y., Kim, Y. H. & Jung, Y. Single-atom catalysts for CO<sub>2</sub> electroreduction with significant activity and selectivity improvements. *Chem. Sci.* **8**, 1090–1096

- (2017).
98. Ju, W. *et al.* Understanding activity and selectivity of metal-nitrogen-doped carbon catalysts for electrochemical reduction of CO<sub>2</sub>. *Nat. Commun.* **8**, 944 (2017).
  99. Bagger, A., Ju, W., Varela, A. S., Strasser, P. & Rossmeisl, J. Single site porphyrine-like structures advantages over metals for selective electrochemical CO<sub>2</sub> reduction. *Catal. Today* **288**, 74–78 (2017).
  100. Genovese, C. *et al.* Operando spectroscopy study of the carbon dioxide electro-reduction by iron species on nitrogen-doped carbon. *Nat. Commun.* **9**, 935 (2018).
  101. Wu, J. *et al.* A metal-free electrocatalyst for carbon dioxide reduction to multi-carbon hydrocarbons and oxygenates. *Nat. Commun.* **7**, 13869 (2016). **The N-doped graphene quantum dots showed a high total CO<sub>2</sub>RR FE of up to 90%, with the C<sub>2</sub> and C<sub>3</sub> product distribution and production rate comparable to those obtained with copper nanoparticle-based electrocatalysts.**
  102. Liu, Y., Chen, S., Quan, X. & Yu, H. Efficient Electrochemical Reduction of Carbon Dioxide to Acetate on Nitrogen-Doped Nanodiamond. *J. Am. Chem. Soc.* **137**, 11631–11636 (2015).
  103. Liu, Y. *et al.* Selective Electrochemical Reduction of Carbon Dioxide to Ethanol on a Boron- and Nitrogen-Co-doped Nanodiamond. *Angew. Chemie - Int. Ed.* **56**, 15607–15611 (2017).
  104. Nakata, K., Ozaki, T., Terashima, C., Fujishima, A. & Einaga, Y. High-yield electrochemical production of formaldehyde from CO<sub>2</sub> and seawater. *Angew. Chemie - Int. Ed.* **53**, 871–874 (2014).
  105. Song, Y. *et al.* Metal-Free Nitrogen-Doped Mesoporous Carbon for Electroreduction of CO<sub>2</sub> to Ethanol. *Angew. Chemie - Int. Ed.* **56**, 10840–10844 (2017).
  106. Huang, J. *et al.* Potential-induced nanoclustering of metallic catalysts during electrochemical CO<sub>2</sub> reduction. *Nat. Commun.* **9**, 3117 (2018).
  107. Kim, Y.-G., Baricuatro, J. H. & Soriaga, M. P. Surface Reconstruction of Polycrystalline Cu Electrodes in Aqueous KHCO<sub>3</sub> Electrolyte at Potentials in the Early Stages of CO<sub>2</sub> Reduction. *Electrocatalysis* **9**, 526–530 (2018).
  108. Kim, Y. G., Baricuatro, J. H., Javier, A., Gregoire, J. M. & Soriaga, M. P. The evolution of the polycrystalline copper surface, first to Cu(111) and then to Cu(100), at a fixed CO<sub>2</sub>RR potential: A study by operando EC-STM. *Langmuir* **30**, 15053–15056 (2014). **An operando EC-STM study showed the surface reconstruction from a polycrystalline Cu electrode first to Cu(111), and then to Cu(100) under CO<sub>2</sub>RR conditions.**
  109. Jiang, K. *et al.* Metal ion cycling of Cu foil for selective C–C coupling in electrochemical CO<sub>2</sub> reduction. *Nat. Catal.* **1**, 111–119 (2018).
  110. Lee, S. Y. *et al.* Mixed Copper States in Anodized Cu Electrocatalyst for Stable and Selective Ethylene Production from CO<sub>2</sub> Reduction. *J. Am. Chem. Soc.* **140**, 8681–8689 (2018).
  111. Singh, M. R., Kwon, Y., Lum, Y., Ager, J. W. & Bell, A. T. Hydrolysis of Electrolyte Cations Enhances the Electrochemical Reduction of CO<sub>2</sub> over Ag and Cu. *J. Am. Chem. Soc.* **138**, 13006–13012 (2016).
  112. Resasco, J. *et al.* Promoter Effects of Alkali Metal Cations on the Electrochemical Reduction of Carbon Dioxide. *J. Am. Chem. Soc.* **139**, 11277–11287 (2017).
  113. Pérez-Gallent, E., Marcandalli, G., Figueiredo, M. C., Calle-Vallejo, F. & Koper, M. T. M. Structure- and Potential-Dependent Cation Effects on CO Reduction at Copper Single-Crystal

- Electrodes. *J. Am. Chem. Soc.* **139**, 16412–16419 (2017).
114. Ayemoba, O. & Cuesta, A. Spectroscopic Evidence of Size-Dependent Buffering of Interfacial pH by Cation Hydrolysis during CO<sub>2</sub> Electroreduction. *ACS Appl. Mater. Interfaces* **9**, 27377–27382 (2017).
  115. Schizodimou, A. & Kyriacou, G. Acceleration of the reduction of carbon dioxide in the presence of multivalent cations. *Electrochim. Acta* **78**, 171–176 (2012).
  116. Dunwell, M. *et al.* The Central Role of Bicarbonate in the Electrochemical Reduction of CO<sub>2</sub> on Gold. *J. Am. Chem. Soc.* **139**, 3774–3783 (2017).
  117. Zhu, S., Jiang, B., Cai, W. & Shao, M. Direct Observation on Reaction Intermediates and the Role of Bicarbonate Anions in CO<sub>2</sub> Electrochemical Reduction Reaction on Cu Surfaces. *J. Am. Chem. Soc.* **139**, 15664–15667 (2017).
  118. Wuttig, A., Yoon, Y., Ryu, J. & Surendranath, Y. Bicarbonate Is Not a General Acid in Au-Catalyzed CO<sub>2</sub> Electroreduction. *J. Am. Chem. Soc.* **139**, 17109–17113 (2017).
  119. Huang, Y., Ong, C. W. & Yeo, B. S. Effects of Electrolyte Anions on the Reduction of Carbon Dioxide to Ethylene and Ethanol on Copper (100) and (111) Surfaces. *ChemSusChem* **11**, 3299–3306 (2018).
  120. McCrum, I. T., Akhade, S. A. & Janik, M. J. Electrochemical specific adsorption of halides on Cu 111,100, and 211: A density functional theory study. *Electrochim. Acta* **173**, 302–309 (2015).
  121. Varela, A. S., Ju, W., Reier, T. & Strasser, P. Tuning the Catalytic Activity and Selectivity of Cu for CO<sub>2</sub> Electroreduction in the Presence of Halides. *ACS Catal.* **6**, 2136–2144 (2016).
  122. Schouten, K. J. P., Pérez Gallent, E. & Koper, M. T. M. The influence of pH on the reduction of CO and CO<sub>2</sub> to hydrocarbons on copper electrodes. *J. Electroanal. Chem.* **716**, 53–57 (2014).
  123. Jouny, M., Luc, W. & Jiao, F. High-rate electroreduction of carbon monoxide to multi-carbon products. *Nat. Catal.* **1**, 748–755 (2018).
  124. Todoroki, M., Hara, K., Kudo, A. & Sakata, T. Electrochemical reduction of high pressure CO<sub>2</sub> at Pb, Hg and In electrodes in an aqueous KHCO<sub>3</sub> solution. *J. Electroanal. Chem.* **394**, 199–203 (1995).
  125. Melchaeva, O. *et al.* Electrochemical Reduction of Protic Supercritical CO<sub>2</sub> on Copper Electrodes. *ChemSusChem* **10**, 3660–3670 (2017).
  126. Rosen, B. A. *et al.* Ionic Liquid–Mediated Selective Conversion of CO<sub>2</sub> to CO at Low Overpotentials. *Science* **334**, 643–644 (2011).
  127. Sun, X. *et al.* Design of a Cu(i)/C-doped boron nitride electrocatalyst for efficient conversion of CO<sub>2</sub> into acetic acid. *Green Chem.* **19**, 2086–2091 (2017).
  128. Goodpaster, J. D., Bell, A. T. & Head-Gordon, M. Identification of Possible Pathways for C-C Bond Formation during Electrochemical Reduction of CO<sub>2</sub>: New Theoretical Insights from an Improved Electrochemical Model. *J. Phys. Chem. Lett.* **7**, 1471–1477 (2016).
  129. Mills, J. N., McCrum, I. T. & Janik, M. J. Alkali cation specific adsorption onto fcc(111) transition metal electrodes. *Phys. Chem. Chem. Phys.* **16**, 13699–13707 (2014).
  130. Deng, Y. & Yeo, B. S. Characterization of Electrocatalytic Water Splitting and CO<sub>2</sub> Reduction Reactions Using in Situ/Operando Raman Spectroscopy. *ACS Catal.* **7**, 7873–7889 (2017).
  131. Dutta, A., Kuzume, A., Rahaman, M., Veszteg, S. & Broekmann, P. Monitoring the

Chemical State of Catalysts for CO<sub>2</sub> Electroreduction: An In Operando Study. *ACS Catal.* **5**, 7498–7502 (2015).

132. Zhu, C. *et al.* In-situ liquid cell transmission electron microscopy investigation on oriented attachment of gold nanoparticles. *Nat. Commun.* **9**, 421 (2018).